Correlating volcanic dynamics and the construction of a submarine volcanogenic apron: an example from the Badenian (Middle Miocene) of North-Eastern Hungary

Di Capua, A.[1,2], Barilaro, F.[2], Szepesi, J.[3,4], Lukács, R.[3], Gál, P.[3], Norini, G.[1], Sulpizio, R.[5,1], Soós, I.[3,6], Harangi, S.[3,6], Groppelli, G.[1]

1. CNR IGAG – Institute of Environmental Geology and Geoengineering, Via M. Bianco 9, 20131, Milan (Italy)

2. University of Insubria, Department of Science and High Technology, Via Valleggio 11, Como (Italy)

3. MTA – ELTE Volcanology Research Group, Budapest (Hungary)

4. Isotope Climatology and Environmental Research Centre (ICER), Institute for Nuclear Research, Hungarian Academy of Debrecen, Debrecen (Hungary)

5. University of Bari "Aldo Moro", Department of Earth and Geoenvironmental Sciences, via Orabona 4, 70125, Bari (Italy)

6. Eötvös Loránd University, Department of Petrology and Geochemistry, Budapest (Hungary)

Abstract

This work studies a submarine volcanogenic apron forming the Nagyhársas Andesite Formation (Badenian – Middle Miocene) in the Mátra Mountains (North-Eastern Hungary), with the aim to identify volcanic processes, from the sedimentary bed scale to the architecture of the whole apron. Fieldwork has been carried out in two different localities (Tar and Sámsonháza villages), where eighteen logs have been measured and correlated, reconstructing the stratigraphic variations of the sedimentary beds and the volcano-sedimentary architectures of the proximal and distal part of the volcanogenic apron. Fifty-two samples have been collected, cut into standard thin sections and petrographically studied to support the interpretation of mechanisms that accumulated the volcanogenic detritus in the submarine realm, as well as to identify the possible volcanic source and how it interacted with the marine environment. The results allow for the first time to underline the importance of a correct interpretation of volcanongenic deposits in the constrain of regional sea level variations, and to discuss the role of active volcanic edifices in shaping the proximal and distal sedimentary architecture of volcanogenic aprons. In proximal areas, the correlation between eruptive cycles and excavation-infill cycles of apron channels suggests that major eruptive events are responsible for channel excavation, whereas minor eruptive events contributed to the infilling of those architectures. In distal areas, the large supply of volcanogenic sediments cannibalizes the sedimentary system, temporally inhibiting the progradation of carbonate platforms nearby the apron offshoots, as well as allows the bypass of topographic barrier (e.g., ridges) favouring mechanisms of sediment spill-over in areas where otherwise sedimentation would be prevented.

Keywords: Nógrád Basin, volcanogenic sedimentation, sea level variations, allogenic controls, cyclicity

1. Introduction

Submarine depositional systems are complex assemblages of sediments emplaced through time under control of the exogenous and endogenous factors. Such a control is exerted at all stages that lead to the accumulation of sedimentary successions, from the generation of sediments, to their transport mechanisms and development of depositional architectures (e.g., Sinclair and Tomasso, 2002; Mutti et al., 2009; Catuneanu et al., 2011; Carey and Schneider, 2011; Schindlbeck et al. 2013; Marini et al., 2015; Henstra et al., 2016; Cunha et al., 2017). Among endogenous and exogenous factors, volcanism is probably one of the most significant, as it is able to provide large volumes of detritus to the sedimentary basins in a short time (e.g., Smith, 1991; Critelli and Ingersoll, 1995; Allen et al., 2007; Manville et al., 2009; Di Capua et al., 2016; Shumaker et al., 2018; Dodd et al., 2020). Volcanism can also produce the accumulation of a wide range of volcanogenic deposits, whose characteristics depend on the parental volcanic events and transport mechanisms (e.g., Trofimovs et al., 2004, 2008; Di Capua and Groppelli, 2016a, b). Furthermore, processes governing the construction of volcanic edifices are often cyclical, with alternated pyroclastic and volcaniclastic deposits that can be identified in the sedimentary records, which link volcanic activity and the evolution of sedimentary basin (e.g., Smith, 1991; Martì et al., 2018; Di Capua and Groppelli, 2018; Bischoff et al., 2019; Di Capua and Scasso, 2020). The integrated analysis of all the above-mentioned processes is critical to improve models on volcano-sedimentary architectures in basins affected by pyroclastic and volcaniclastic deposition.

This study presents the reconstruction of stratigraphy of a submarine volcanic apron accumulated in the Pannonian basin during Miocene and exposed in the Mátra Mountains (North-Eastern of Hungary – Fig. 1). Lithostratigraphy, microscopic textures and petrography of the sedimentary record have been analysed and compared to discuss: 1) the mechanisms leading to the generation, transport and underwater accumulation of the volcanogenic beds; 2) the provenance of the detritus and possible multiple volcanic sources; 3) the relationship between eruptive cycles and the development of architectural elements; 4) the relationship between stages in the activity of the volcanic source and corresponding features of the proximal part of the apron; 5) the interaction among volcanism, sedimentary processes and seafloor topography in the development of the apron offshoots; 6) the importance of the correct interpretations of volcanogenic sequences in the reconstruction of regional sea level variations.

2. Geological Setting

The Pannonian basin developed by considerable thinning of the continental lithosphere during the Miocene in an area bounded by the orogenic belts of the Alps, the Carpathians and the Dinarides (Horváth et al., 2015). The rifting started west-southwest at about 22 Ma and propagated towards east up to ca. 8 Ma (Balázs et al., 2016). The significant extension of the lithosphere was accommodated by suction effect of the retreating subduction along the eastern Carpathians (Royden et al., 1982; 1983; Csontos et al., 1992). The complex tectonic evolution was accompanied by intense volcanism characterized by eruptions of wide range of magmas (from basalts to rhyolites; Szabó et al., 1992; Harangi, 2001; Seghedi et al., 2004; 2005; Pécskay et al., 2006; Harangi and Lenkey, 2007; Seghedi and Downes, 2011). The onset of extension in the north-northeast part of Pannonian basin was associated with large caldera-forming eruptions of silicic magmas from 18 Ma to 14 Ma (Lukács et al., 2015; 2018). Pyroclastic deposits of these explosive volcanic events covered the surface of the major part of the Pannonian basin and therefore, they are important key-horizons in the Miocene stratigraphy, like the Tar Dacite Tuff Formation (TDF) of Figure 1. This volcanism was partly contemporaneous with calc-alkaline andesitic to rhyolitic volcanic activity yielding a chain of volcanoes from west to east in the northern part of the Pannonian basin from ca. 16 Ma to 10 Ma, like the Hasznos Andesite Formation (HAF) and the Nagyhársas Andesite Formation (NAF) of Figure 1 (Downes et al., 1995; Harangi et al., 2001; 2007).

The diachronous lithospheric extension of the Pannonian basin formed several subbasins, mostly half-grabens (Tari et al., 1992; 1999; Fodor et al., 1999) that were filled first by the large inland sea of the Paratethys and then the Pannon lake (Magyar et al., 1999; Rögl, 1999). One of them (the Nógrád Basin) developed in the northern part of the Pannonian basin system along the NNE-trending Zagyva trough (ZT) (Hámor, 1985; Tari et al., 1992; Fodor et al., 1999; Püspöki et al., 2017). In the study area, the trough is delimited to SW by the Zagyva Fault (ZF), which separated it from the Mátra Volcanic Complex, and to NE by a fault here named as Sámsonháza Fault (SaF), which separated it from the Zagyva ridge (ZR). This latter element is a horst with an elongation of SE to NW, bordered to SW by the SaF and to NE by the Szentkút fault (SzF) (Fig. 1A - Hámor, 1985; Püspöki et al., 2017).

The progressive subsidence of the ZT, coupled with frequent sea level variations, controlled the evolution of the sedimentary record in the Nógrád basin (Figs. 1A and B), which opened with the accumulation of deep-water sediments since the Karpatian (Garáb Schlier Formation - GSF). Above the GSF, a regressive, shallow marine sequence occurs (Fót Formation - FF), immediately overlain by the submarine volcanogenic deposits of the HAF (Vakarcs et al., 1998; Póka et al., 2004; Püspöki et al., 2017). This volcano-sedimentary cycle is overlain by the TDF (Fig. 1B), a thick pyroclastic sequence emplaced by multiple eruptive events, partially subaerially and partially in shallow marine environments (e.g., Hámor, 1985; Karátson et al., 2001; Lukács et al., 2018). The TDF is one of the more prominent stratigraphic key-horizon in the Pannonian basin. The age of the volcanic event was formerly considered to fall at the boundary between the Karpatian and the Badenian time (16.4 Ma - e.g., Hámor et al., 1980; Vakarcs et al., 1998). However, Lukács et al. (2015; 2018) determined the age of the TDF at ~14.9 Ma by zircon ID-TIMS technique and concluded that the TDF can be correlated with the eruption of the Demjén ignimbrite in the Bükkalja area (NE of Hungary). Above the TDF, the Nagyhársas Andesite Formation (NAF) was emplaced between 14.9 and ~14 Ma and form the massive Mátra and Cserhát volcanic complexes (e.g., Karátson et al., 2001; Póka et al., 2004). The NAF comprises terrestrial and subaqueous deposits. The terrestrial sequences form most of the volcanic morphologies and deposits of the Matra Volcanic Complex, whereas the subaqueous part of the NAF is exposed in the Nógrád Basin (e.g., Karátson et al., 2001; Póka et al., 2004; Nagymarosy and Hámor, 2013). There, the NAF is intercalated by the transgressive fossiliferous, clastic to calcareous deposits of the Pécsszabolcs Limestone Member (PLM), Early Badenian in age (Fig. 1B). On top, it is erosively overlain by the clastic to calcareous deposits of Rákos Limestone Member (RLM), Late Badenian in age (Fig. 1B). Both Members are part of the Leithakalk Formation (LF) (Gyalog, 2005; Pelinkan and Ronai, 2005; Prakfalvi, 2005; Nagymarosy and Hámor, 2013).

3. Methodology

Stratigraphic logs have been compiled through a geological survey in two different areas, near the villages of Tar and Sámsonháza (Fig. 1C) with the aim to constrain the paleoenvironment where the volcanogenic deposits were emplaced. On the NAF, eighteen logs have been measured near the village of Tar on top of an abandoned quarry and along two parallel creeks, and near the village of Sámsonháza in an ancient quarry and 1.3 km to NE of it (Figs. 1 and 2). A total of fifty-two samples have been collected and cut into standard thin sections for compositional and textural analyses. The combination of stratigraphic and petrographic results has been used to define nine facies. Measured logs have been correlated through key features, including the marker beds defined by similar petrographic and stratigraphic features, erosive surfaces and formations' boundaries. Six facies associations (three in Tar and three in Sámsonháza) have been defined on the base of the spatial facies distribution and subsequently correlated together to reconstruct the stratigraphic architectures characterizing the NAF in the study area.

4. Stratigraphy of the NAF in the Zagyva Trough

Figure 1C shows the general stratigraphy of the study area as documented during fieldwork. In the Tar area, fieldwork documented that the NAF closes a volcano-sedimentary sequence, opened by almost 10 m of submarine marl deposits ascribed to the Garáb Schlier Formation. This Formation is overlain by a *ca.* 10 m chaotic to bedded andesite tuff-breccias and tuffs that belong to the submarine HAF. Above it, an almost 30 m-thick rhyodacitic ignimbrite deposit of the TDF is exposed below the studied sedimentary sequence. Where documented, the contact between the TDF and the upper NAF is erosional and scour directions have been measured (Fig. 2). In the Sámsonháza area, the studied sequence has been logged in three main sites named SA, in the Zagyva Trough, SB and SC, on the Zagyva Ridge (Fig. 1A). In this area, fieldwork revealed that the NAF is included between the TDF at the bottom and the RLM on top. In site SA, the NAF crops out 10 m above the top of the TDF and could be followed up until its top. It is composed of a volcanogenic sequence, interbedded by a thin marly limestone layer of the PLM at the bottom, and two concordant andesite layers on top (Fig. 3A). The contact between these andesite bodies and the clastic sequence is fluidized (Fig. 3B), therefore the andesite bodies are interpreted as sills in disagreement with previous authors who consider them as lava flows (e.g., Nagymarosy and Hámor, 2013). The uppermost andesite sill caps the NAF and is erosively overlain by the carbonate sequence of the RLM (Fig. 3C). In site SB, the NAF has a limited thickness of 5 m, comprised between the TDF and the RLM. Site SC is the only place where the contact between the TDF and the NAF (not erosive) is visible.

5. Facies description and interpretation

Fieldwork and petrographic analyses allowed the identification of nine facies, described and interpreted in terms of sedimentation mechanisms, and correlated to the TDF, NAF and PLM through petrographic features.

5.1 Facies A

Field description: Facies A has been observed in Tar exposed along a hummock, dipping toward SE in site A and toward NW in site B. It consists of two units: a basal ungraded ash layer, almost 1 m-thick, and an upper monomictic moderately sorted, matrix- to clast-supported, normally graded lithic breccia layer, almost 3 m-thick (Fig. 4A). Weak wavy stratification characterizes the deposits and, along it, many blocks and megablocks (up to 2 m) are aligned. Megablocks often present jigsaw cracks (Fig. 4B), some of which are open and filled up by ash matrix and minor small angular blocks, forming diapiric flame-like structures with sigmoidal-shaped laminae running parallel to the fracture walls (Fig. 4C). Some blocks are flattened and completely broken (Fig. 4D).

Petrographic description: Facies A matrix is mainly composed of loose phenocrystals of plagioclase (Fig. 4E), irregular to rounded pumices (Figs. 4E and F), and rare black scorias with micrometric laths of plagioclase (Fig. 4G). All the particles are dispersed in a vitric, locally highly vesiculated groundmass that shows colours ranging from yellow to dark brown. Vesicles have glassy rims, sometimes palagonitized, and are rarely filled up by fine ash (Figs. 4E and F). Pumices are often deformed forming a continuum with the groundmass (Fig. 4F). Intergranular contacts among the scoriaceous particles are generally constituted of glass, which locally shows palagonitization (Fig. 4E). Megablocks and blocks observed in the field show a banded fluidal texture, locally embedding phenocrystals of plagioclase (Fig. 4H), but are never observed as a constituent of the matrix deposits.

Interpretation: geometry and sedimentological structures (ungraded to normally graded breccia) of Facies A are akin to those of block and ash flow (BAF) deposits (Schwarzkopf et al., 2005). The basal ash unit of the BAF corresponds to the basal shear zone of Cardona et al. (2020), characterized by a high shear stress (Branney and Kokelaar, 2002). Groundmass vesiculation highlights that gases trapped as pore fluids among the particles lowered the internal friction resistance to flow deriving from the intraparticle collisions. The upper normally graded part includes blocks and megablocks colliding among each other while rafting on top of the flow (De Blasio and Elverhoi, 2011). Deformation and breakage of blocks, generated by differences in stress applied to different parts of the block, were enhanced by collision during the flowage (e.g., Ui et al., 1986). Once the flow decreased its velocity, blocks induced overpressure over the underlain ash, which was squeezed upward intruding the space between blocks (Branney and Kokelaar, 2002; Douillet et al., 2015; Roverato et al., 2018). Groundmass palagonitization occurred soon after the BAF emplacement, and highlights water circulation inside the still hot deposit. This also indicates that BAF was accumulated in a submarine realm.

5.2 Facies B

Field description: Facies B corresponds to reverse graded tuff-breccias (Fig. 5A). These beds are generally matrix-supported at the base and become clast-supported on top (Fig. 5B-C). The grey matrix is composed of fine ash, but occasionally becomes coarser. Blocks are angular to subangular, rarely sub-rounded, and are mainly represented by lava blocks composed of phenocrysts of plagioclase and pyroxene in a massive to vesiculated, red to green groundmass. Very rare accidental rhyodacitic blocks have also been observed. Among the lava blocks, the most representative lithotype is green massive lava (50-60%), followed by red lavas (20-32%) dark green lavas (14-20%), and light green lavas (1-6%). Blocks have mean size around 10 – 12 cm, with a maximum dimension of 70 cm (a red lava block).

Petrographic description: Facies B appears poorly sorted and mainly composed of lithics and minor loose crystals of plagioclase and clots of pyroxene, surrounded by a brown to dark brown microcrystalline groundmass (Figs. 5D-I). The lithic fraction comprises particles with irregular, ameboid and rounded shapes made of porphyritic lavas, with phenocrystals and clots of plagioclase and minor pyroxene, embedded in a grey, pale brown or brown microcrystalline groundmass (Figs. 5D-E). In some cases, lava fragments present vesicles rimmed by palagonite (Fig. 5E). Many particles are characterized by a light-yellow reaction rim of weathered glass (Figs. 5D, 5E, 5H and 5I), whereas minor lithics show a pale brown reaction rim (Fig. 5H). Groundmass is partially impregnated by a yellow to brown cement of phyllosilicates and palagonite, grown onto the previous glass (Figs. 5E and 5H). Palagonite and phyllosilicates also form veins that crosscut the lithics and substitutes their internal glassy groundmass (Figs. 5D and 5G).

Interpretation: Reverse grading and large amounts of angular and subangular blocks similar in mineralogical compositions indicate that Facies B deposits were accumulated by BAFs dominated by a granular flow regime (Sulpizio et al., 2014). Texture differences documented among blocks suggest that the probable source of such BAFs was a complex lava dome with different internal fabrics (e.g., Zavada et al., 2009; Szepesi et al., 2019). Few rounded blocks and rhyodacite blocks have been probably eroded from the substratum during the BAF motion and incorporated into the final deposits (e.g., Trofimovs et al., 2008; Di Capua and Scasso, 2020). Reaction rims, yellow to brown cement and fracturing/weathering of lithics indicate that post-emplacement water circulation occurred when particles were still hot, favouring hydrothermal reactions that transformed the glassy components into phyllosilicates/palagonite (McPhie et al., 1993; Di Capua and Groppelli, 2016b).

5.3 Facies C

Field description: Facies C comprises amalgamated strata of polymictic tuff-breccias, lapilli-tuffs and tuffs, in metric to plurimetric layers (Figs. 6A – E). The coarser layers are generally massive or weakly laminated, with elongated blocks parallel to the lamination or accumulated in pockets (Fig. 6A). The finest parts of the deposits are massive, parallel to wavy or cross-bedded laminated, but laminations are generally truncated (Figs. 6B and C). Pluricentimentric blocks are frequently dispersed in the deposits. Some of them present ball and pillow structures at their bottom and are characterized by flanks and top onlapped by the surrounding sediments (Fig. 6D). Although intermediate lava fragments and scorias are the most representative particles in the detritus, lapilli- to ash-size subrounded pumices arranged in pluricentimetric thick, metric wide dune structures (Fig. 6E) has been frequently observed (e.g., Log 8 - Fig. 2).

Petrographic description: Facies C includes two distinct petrofacies named C1 and C2. Petrofacies C1 is mainly composed of detritus intermediate in composition (plagioclase + pyroxene; plagioclase). The coarse-grained beds of this facies are clast-supported layers almost entirely composed of sub-rounded lithics, with rare loose crystals of plagioclase. Particles within the beds are coarse, subangular to subrounded in shape and rimmed by devitrified glass and dark brown palagonite (Figs. 6F-G). In addition, brown palagonite also substitutes most of their glassy textures (Fig. 6F). Groundmass among particles is well developed in coarser beds, showing a microcrystalline texture embedding µm-scale laths of plagioclase (Fig. 6G). In finer beds, groundmass becomes highly vesiculated, with vesicles elongated in shape and rarely filled up by palagonite (Fig. 7A). It wraps lathwork and porphyritic lava fragments, dark orange scoriae, loose crystals of plagioclase and clots of clinopyroxene with vesicles rimmed by palagonite (Figs. 7B-D). As shown in Figure 7D, particles are also often rimmed by dark brown to grey devitrified glass and may have green zeolites grown on plagioclase crystals (Fig. 7D). Other lava fragments have an ameboid shape, and they are characterized by frequent palagonite that substitutes the vitric groundmass without obliterating the primary vesiculation (Figs. 7E - 7H).

Petrofacies C2 has been observed only in few deposits directly overlaying the TDF (Fig. 2 – Log 1), and includes beds almost entirely composed of highly vesiculated rhyolitic fragments, loose crystals of quartz, plagioclase, sanidine and biotite, and rare accidental lava fragments intermediate in composition, all embedded in a grey, microcrystalline to cryptocrystalline groundmass (Figs. 7I-K). Fluidal structures, consisting of glass weathered into clay, rarely wrap particles (Fig. 7I). Plugs of well sorted particles (Fig. 7J) and gas pipe-like structures, formed by vertical well sorted particles and a dark brown cement (Fig. 7K), have been rarely documented.

Interpretation: Massive appearance, truncated erosion surfaces and dune accumulation result from repetitive deposition, erosion and self-channelization of high- to low-concentrated unsteady flows generated by PDCs (Douillet et al., 2013, 2018). Flow-boundary conditions influenced the microscopic textures of the beds: when fluid-escape worked efficiently, fines were depleted by the flow, the flow lost its concentration and the resulting deposits are well sorted (Branney and Kokelaar, 2002). When flow-boundary conditions were traction-dominated, gases still entertained within the high-concentrated flows and fines were not elutriated (Branney and Kokelaar, 2002; Sohn et al., 2008). Largest blocks are interpreted as ballistics and ball and pillow structures resulted from their impact on the underlying beds (Douillet et al., 2015). Once settled, the submarine water circulating in the deposits reacted with the still hot particles, favouring the partial sintering of rims and vitric groundmass (when present), as well as the subsequent palagonitization of the glass (McPhie et al., 1993; Wadsworth et al., 2014; Di Capua and Groppelli, 2016b). Deposits characterized by petrofacies C2 probably represent the final phase of the TDF emplacement.

5.4 Facies D

Description: Facies D includes moderately sorted, matrix-supported, massive, rarely reverse-graded lapilli-tuff and tuff deposits (Figs. 8A and B). Thickness ranges between 10 and 100 cm. Accidental outsize (maximum 100 cm) lithics are frequent and have a rhyodacitic composition in both study areas. In Tar, angular to subrounded lithics of more intermediate nature are also present.

Petrographic description: Facies D is largely composed of vesiculated scoriae and lava fragments, intermediate in composition, with loose crystals of plagioclase in minor amount (Figs. 8C-G). Scoriae and lithics are mainly irregular (Figs. 8B and C) and ameboid in shape (Fig. 8F), with minor sub-rounded particles (Fig., 8E), and show groundmass that varies from porphyritic to microcrystalline in textures, from yellow, red to black in colour (Figs. 8C-G). All the particles are generally rimmed by glass and/or palagonite (Figs. 8B and 8D). Deposit groundmass is mainly glassy to microcrystalline (Figs. 8B and 8D) and is often palagonitized (Figs. 8B-D). Vesiculation is diffuse in all samples, with vesicles rimmed by glass and palagonite (Figs. 8F and 8G). In Sámsonháza (Fig. 2 – Log 18), rare fragments of obsidian, showing a glassy fluidal texture embedding crystals of quartz, have also been observed (Fig. 8H).

Interpretation: The absence of grading, the massive aspect of the deposits and its moderate sorting indicate that Facies D was accumulated by PDCs, whose motion was sustained by a fluid-escape dominated regime (Branney and Kokelaar, 2002). The recognition of a good degree of hydrothermal weathering within the groundmass reveal that all deposits were accumulated by hot flows that interacted with water (McPhie et al., 1993; Sohn et al., 2008). Provenance of obsidian detritus is discussed in paragraph 7.1.

5.5 *Facies E*

Field description: Facies E groups together all those deposits that are characterized by a reverse to normal grading, which has been observed in both areas (Figs. 9A). The stratigraphy comprises a basal medium sandy layer, overlain by a coarser main body, and a muddy, weakly laminated to massive layer. Traction carpets and grain-size variation are rarely observed in the central layer of the deposits. All the deposits are composed of intermediate detritus, which generally shows a porphyritic texture, with phenocrystals of plagioclase, and are sometimes vesiculated. In the Sámsonháza area, rounded pumices are sometimes included in these deposits.

Petrographic description: Facies E includes deposits mainly composed of intermediate lava fragments, pumices and loose crystals of plagioclase (Figs. 9B – G). Lithics are often ameboid in shape (Figs. 9B-D) and show a yellow to brown porphyritic groundmass with phenocrystals of plagioclase. Pumices can wrap phenocrystals of plagioclase (Fig. 9C), and often create a continuum with the microcrystalline groundmass, becoming undistinguishable from it (Figs. 9B and 9F). Vesicles are rarely rimmed by glass or filled by zeolites (Figs. 9B and 9F). Groundmass is generally microcrystalline, as shown in Figs. 9D and 9E. Yellow to dark yellow patches on it indicate that it has been subsequently weathered into palagonite. These patches also grew onto the glassy parts of the lithics. As shown in Fig. 9G, particles can also be rimmed by yellow to dark brown palagonite. In a deposit of Sámsonháza (upper part of Log 14 – Fig. 2), a lava fragment ascribable to the megablocks of Facies A (*cfr* Fig. 4H), characterized by palagonitized rimmed vesicles, has been observed (Fig. 9G).

Interpretation: Facies E includes deposits accumulated by concentrated density flows, in which the basal part moved supported by grain-to-grain interaction, favouring the elutriation of fines later accumulated as fallout (Mulder and Alexander, 2001; Branney and Kokelaar, 2002). Rimmed particles and rimmed vesicles, together with palagonite, indicate a strong interaction between the hot detritus and the surrounding water. Therefore, these flows, accumulated as turbidity currents *sensu lato*, were generated by the disaggregation of PDCs in the submarine realm (e.g., Trofimovs et al., 2008; Di Capua and Groppelli, 2016a).

5.6 *Facies F*

Field description: Facies F comprises normally graded matrix- to clast-supported deposits of volcanogenic sandstones (Fig. 10A). Matrix of the lowermost deposit in Tar (Log 11 – Fig. 2) is composed of rhyodacitic detritus, with rare rounded accidental lithics (up to 80 cm) of lavas intermediate in composition, volcaniclastic sandstones and minor ignimbrite, sometimes arranged in traction carpets. All the other beds are characterized by matrix with an intermediate composition. Outsize accidental rounded blocks of ignimbrite (50 cm) are documented in two beds of Sámsonháza (Log 15 – Fig. 2).

Petrographic description: Facies F comprises two different petrofacies, named F1 and F2 and defined on the base of the mineralogical composition of their detritus. Petrofacies F1 groups all those beds constituted by detritus intermediate in composition (Figs. 10B-F), and includes ameboid, irregular to subrounded porphyritic lava and scoria fragments with plagioclase and minor pyroxene as phenocrystals, irregular to flattened pumices, in case wrapping phenocrystals of zoned plagioclase and pyroxene, loose crystals of angular plagioclase (Fig. 10D). At Sámsonháza (Log 15 - Fig. 2), rare fragments of obsidian have been also documented (Fig. 10G). Groundmass has a light brown colour and is characterized by a pervasive palagonitization (Figs. 10B and C).

Petrofacies F2 is documented for that bed directly overlaying the TDF in Log 11 (Fig. 2). It is composed of a lithic fraction that includes vesiculated rhyodacitic fragments with a fluidal texture, ascribable to the TDF, shards, rare lithics with lathwork texture and phenocrystals of plagioclase, and a loose mineral fraction of quartz, plagioclase, biotite and minor sanidine (Figs. 10H and 10I). Grey groundmass is cryptocrystalline, locally weathered into clay.

Interpretation: The subsequent accumulation of massive sand, laminated sand, and massive mud reflects changing flow regimes, passing from granular, to traction-domitated (e.g., Mulder et al., 2001; Sulpizio et al., 2014). This transformation finds correspondence in the superimposition of facies F5, F7 and F9 of Mutti et al. (2003) in flows that passes from concentrated density flows to turbidity flows due to the decrease in density (Mulder and Alexander, 2001; Pierce et al., 2018). This change is controlled by the decrease in particle concentration that occurs during the motion of the flows. The uppermost and finest part collects particles elutriated during the flow and settled down by direct fallout (Branney and Kokelaar, 2002; Trofimovs et al., 2008; Di Capua and Groppelli, 2016a). When the concentration is still enough to sustain grain-to-grain collision flow mechanisms, currents can become erosive and incorporate loose detritus along its path (Di Capua et al., 2016). Differences in detritus composition are indicative of different magmatic source that generated the flows. It is probable that the lower deposits, rhyodacitic in composition, had genetic relationship with the TDF. Absence of vesiculation and low- to no-grade of weathering, together with the presence of fresh shards and rounded accidental lithics differing in dimensions, indicates that they were accumulated by lahars (Di Capua and Scasso, 2020) that reworked the loose rhyodacitic deposits of the TDF. On the contrary, the abundant weathering occurring in the flows intermediate in composition highlights that they were generated by PDCs that mixed with sea water during their motion and transformed into water-supported flows (e.g., Trofimovs et al., 2008; Duraiswami et al., 2019). Provenance of obsidian detritus is discussed in paragraph 7.1.

5.7 Facies G

Field description: Facies G has been recovered only at Sámsonháza (Logs 14 and 15 – Fig. 2). It is constituted by well sorted, massive layers characterized by the large amounts of angular pumices, sometimes mixed with normally graded dark grey to black scoriaceous lava fragments (Fig. 11A).

Petrographic description: matrix-free samples of Facies G are characterized by pumices and scoriaceous fragments showing a good degree of palagonitization (Fig. 11B). Pumices are also characterized by rimmed vesicles (Fig. 11C). Scoriaceous fragments are generally composed of a dark grey to black matrix (Fig. 11B), with small laths of plagioclase embedded in a massive matrix. In addition, on top of Log 15 (Fig. 2), a scoriaceous fragment characterized by a fluidal texture wrapping laths of plagioclase, with vesicles rimmed and/or palagonitized, has been recovered (Fig. 11D). Petrography and texture of such fragments are alike to those of megablocks in Facies A (Fig. 4H).

Interpretation: Facies G includes fallout deposits, as indicated by the large abundance of angular pumices. Glassy rims and glass palagonitization indicate that pumices were still hot when entering the water, and consequently rapidly sank without rafting. This accords to field and experimental data (Jutzeler et al., 2016; Fauria et al., 2017) demonstrating that hot and large pumices are generally prone to rapid sink unlike cold pumices, which in turn raft away. The presence of scoriaceous fragments with petrography and texture alike to those of Facies A blocks suggests that Sámsonháza area was downwind with respect to the volcanic source.

5.8 Facies H

Field description: Facies H comprises thin, muddy deposits (Fig. 12A), characterized by weak wavy laminations. Each single lamina is generally well sorted, and the coarse-grained laminae are often matrix-free.

Petrographic description: Facies H is characterized by alternations of submillimeter (hundreds of µm) to micrometer particles, sometimes show a normal grading, packaged in parallel laminations (Fig. 12B). Particles included are loose minerals of plagioclase and pyroxene, dark intermediate lithics with rare phenocrystals of plagioclase and glassy fragments (Figs. 12C-F). Glass, replaced by amorphous palagonite, commonly embeds single particles or fills the intergranular porosity (Figs. 12D-F).

Interpretation: Facies H deposits were accumulated by direct fallout (Mulder et al., 2001) of hot detritus, as testified by the intense palagonitization. Unlike Facies F, these deposits are the very distal tails of disaggregated PDCs (*cfr* Trofimovs et al., 2008).

5.9 Facies I

Field description: Facies I includes a layer cropping out in the Sámsonháza quarry (Log 14 – Fig. 2). It is constituted of very fine, massive, grey, fossiliferous marly limestone (Fig. 13A). Fossil content includes bivalves (Fig. 13B) and gastropods (putative *Cirsonella* - Fig. 13C).

Petrographic description: Microscopic analyses reveal that the layer is characterized by a micrite matrix embedding few fragments of porphyritic lavas (Fig. 13D), single minerals of plagioclase and quartz (Fig. 13E), as well as fossils (Fig. 13F). Volcanic fragments and minerals are often substituted by secondary, obliterating sparry calcite (Fig. 13G).

Interpretation: this massive and fine grain size layer is a wackestone according to Dunham (1962) and is alike to those described by Randazzo et al. (1999) in the PLM.

6. Facies association and depositional architectures

6.1 Facies Associations

Based on the spatial distribution of the nine facies six facies associations (three in Tar and two in Sámsonháza) have been identified (Figs. 14 and 15).

6.1.1 Facies Association 1 (FA1)

Description: FA1 has been documented in Tar and groups together beds of Facies A, B and C, with rare drapes of Facies E and G. In site A, FA1 is observed at the bottom of Logs 2 and 4 (Figs. 14A and 15). In Log 2, coarse amalgamated beds of Facies C are erosively overlain by a thick deposit of Facies A and other fine amalgamated deposits of Facies C. Field evidences indicate that this sequence was accumulated in a scour excavated into rhyodacitic deposits of Log 1 (Figs. 2 and 15). In Log 4, FA1 is represented by amalgamated fine deposits accumulated at the bottom of a channel, with dispersed pluricentimetric blocks on the channel floor. In site B, FA1 includes Facies A, B and C of Logs from 5 to 8 and Log 10. In Logs 5 and 6, FA1 is again represented by the sequence Facies C, A, C, in which Facies A erosively overlain the lowermost deposits, but all the layers are thinner and finer rather than those of site A. In Log 7, FA1 comprises a thick deposit of amalgamated layers, mainly ashy in grain size, with blocks aligned along NW-trending bedforms. In Log 8, FA1 erosively overlies deposits of Facies D, and is composed of amalgamated strata of Facies C, mainly blocky in grain size, intercalated by a layer of Facies E. Wavy bedforms have been observed in an ash-size layer (Figs. 14B and 15). In the uppermost Log of this site (Log 10), FA1 is represented by thin layers of Facies B and C, interdigitated with layers of other Facies Associations. In site C, FA1 is documented in Logs 12 and 13, and is mainly composed of thick deposits of Facies B, rarely intercalated by thin drapes of Facies G. The bottom of FA1 in Log 13 is erosive.

Interpretation: FA1 includes deposits that open the channel sedimentation, accumulated in the lows of the channel surfaces (e.g., Shanmugam and Moiola, 1988; Covault et al., 2016). From a volcanological point of view, FA1 reflects moments of intense and particularly destructive volcanic activity, such as dome collapses, resulting in the accumulation of very thick and very coarse deposits such as those of Facies A, B and C. The different superimposition of Facies is the result of the type of eruptive event and how it evolved during time.

6.1.2 Facies Association 2 (FA2)

Description: FA2 appears in all the Tar logs with beds, mainly tabular, of Facies from D to G (Fig. 15). In site A, it includes a single reverse-to-normal graded thick deposit of Facies E, overlain by thin deposits of Facies D and rare drapes of Facies E and F (Log 2). In Log 3, FA2 is characterized by a thickening and coarsening upward sequence that includes layers of Facies D, E and F. This sequence is also bounded at the bottom and on top by erosional channel surfaces. In Log 4, FA2 includes a thick deposit of Facies D, which overlies the lower amalgamated sequence included in FA1. In site B, FA2 appears in Log 7 overlaying an erosional surface with thin layers of Facies B and D, which are laterally equivalent to a thick layer of Facies A included in FA1. FA2 also groups layers of Facies D and G on top of Log 7. In Log 8, FA2 is represented by a thin, lapilli-size layer of Facies D, erosively closed up by a sequence of FA1. In Logs 9 and 10, FA2 groups thin lapilli-tuff deposits. In site C, FA2 has been detected in Log 12 as characterized by reverse-graded layers typical of Facies D and lapilli- to ash-size layers of Facies F. In Log 13, FA2 has a higher variability in terms of Facies, including thinning upward beds of Facies B, and lapilli- to ash-size layers of Facies D and F.

Interpretation: FA2 groups together packages of medium to fine-grained deposits that generally mantle those of FA1, therefore constituting the later stage of channel-fill sedimentation (e.g., McHargue et al., 2011). From a volcanological point of view, FA2 includes deposits accumulated by a less catastrophic and powerful volcanic activity when compared with FA1. This is indicated by the accumulation of medium to thin and medium to fine grain size deposits of Facies from D to G. In this scenario, the amounts of detritus supplied by the transformation of PDCs moving underwater (Facies E and F) becomes important (e.g., Di Capua and Groppelli, 2018; Di Capua and Scasso, 2020).

6.1.3 Facies Association 3 (FA3)

Description: FA3 is composed of all those Facies C and F with petrofacies C2 and F2, always detected at the boundary between the TDF and the NAF (Fig. 15). Therefore, it includes all the beds of Log 1 and the basal layer of Log 2 ascribed to Facies C, as well as a single layer of Facies F deposited into a channel structure, as depicted in Log 11 (Fig. 15).

Interpretation: these channel-fill deposits were accumulated (soon) after the TDF settling on the erosional surface on top of the TDF deposit.

6.1.4 Facies Association 4 (FA4)

Description: FA4 has been documented in site SA of Sámsonháza (Figs. 14C and 15). It includes beds of Facies from D to F, with single beds of Facies B, G and H intercalated (Logs 14 and 15). Most of the beds of Facies F are characterized by a coarse lapilli-size basal unit, which passes upward to an ashy to fine ashy unit. In Log 14, these beds are a thinning-then-thickening upward, characteristic that is weakly replicated in beds of Log 15. Beds of Facies D are rare and ashy with rarely dispersed blocks. It has been observed that different beds have a convex shape, pinching out laterally (Fig. 14C).

Interpretation: The geometrical arrangement of FA4 deposits, characterized by a nested offset stacking with beds that pinch out laterally one against the other, indicates that the deposit was accumulated in a confined sub-environment (Henstra et al., 2016).

6.1.5 Facies Association 5 (FA5)

Description: FA5 has been observed in all the Sámsonháza sites (Fig. 15). In site A, it characterized the upper part of Log 15 and the entire Log 16, composed of thin to thick tabular beds of Facies D and F, with rare drapes of Facies E intercalated. In site B, where the thickness of the NAF is reduced to 5 m, FA5 includes thin beds of Facies F on top of the sequence. In site C, FA5 overlays the TDF with two layers of Facies D.

Interpretation: Deposits of FA5 are sheet-like deposits accumulated in a relatively unconfined sub-environment (Etienne et al., 2012; Henstra et al., 2016).

6.1.6 Facies Association 6 (FA6)

Description: FA6 includes only the thin layers of Facies G accumulated in Sámsonháza site B (Log 17 – Fig. 15).

Interpretation: deposits of facies FA6 are accumulated in confined and unconfined environments as fallout.

6.2 Depositional Architecture of the NAF in the Nógrád Basin

The studied areas of Tar and Sámsonháza are characterized by distinctive Facies Associations and architectural elements that allow the identification of sub-environments where volcanogenic detritus was accumulated (Figs. 15 and 16).

The stratigraphy of Tar is dominated by the superimposition of channels with an incising-to-aggrading vertical trajectory that progressively migrated toward NE. This kind of accretionary behaviour is typical of turbidite systems (Jobe et al., 2016). All the observed channels are filled and characterized by low rate of overbank aggradation and low accumulation of very fine-grained drapes. The stratigraphic sequence of these channels is composed of thick layers of FA1 overlain by thinner layers of FA2 (Fig. 15), truncated upward by the subsequent channel basal surface. FA1 includes pyroclastic breccias and amalgamated sequences, which are all typical of channel axes (McHargue et al., 2011; Covault et al., 2016; Li et al., 2016). The finer deposits of FA2 are, instead, layers that could identify axis, off-axis and margin elements, on the base of their stratigraphic position. Most of the logged layers of FA2 are channel axis deposits that overlie FA1 beds, such as those of Logs 2, 7, 12 and 13. Reduced thickness (Log 4) and rapid succession of coarse and fine deposits

(Log 13) identify the off-axis elements of channels in site A and C (McHargue et al., 2011). FA2 layers of Log 3, deposited directly on a channel erosional surface, are interpreted as deposits of a lateral migrating margin (Covault et al., 2016). On a larger scale, the presence of Facies A, B and/or C as channel-fill deposits allows the identification of two main channel systems. The first channel system (A) includes channels of sites A and B, where the sedimentation is opened by thick sequences of Facies A and C, overlain by finer and thinner beds, whereas Facies B is extremely rare. The second channel system (B) is that of site C, located to the west with respect to the first one. Here, beds of Facies B are preponderant, whereas no layers of Facies A and C have been documented.

The stratigraphy of Sámsonháza is dominated by three lobe architectural elements (lobe axis, off-axis and fringe lobe), defined through the characterization of the bed arrangement of FA4, FA5 and FA6 (Figs. 15 and 16). The first architectural element (lobe axis) is defined by beds arranged in a thinning-then-thickening upward, pinching out laterally (Prélat et al., 2009; Kane and Pontén, 2012; Prélat and Hodgson, 2013). This upward becomes an off-axis (second architectural element), characterized by beds of FA5 deposited in an unconfined environment, with 1) a general thickening upward trend like in Log 16, or 2) a constant thickness like at the base of Log 14, as well as in Logs 17 and 18 (Etienne et al., 2012; Prélat and Hodgson, 2013; Henstra et al., 2016). Fringe lobe deposits (third architectural elements) are identifiable in the fine and thin beds at the base of Log 17 (FA6) (Prélat et al., 2009; Kane and Pontén, 2012). Due to its different sedimentary nature, the bed of Facies I recovered in Log 14 and ascribable to the PLM represents an interlobe deposit (Prélat et al., 2009), accumulated during a quiescence in the volcanic activity (Randazzo et al., 1999).

7. Discussions

7.1 Signatures of volcanogenic detritus and related sources

The stratigraphic and petrographic data identify three main signatures of the volcanogenic detritus. The first signature is preponderant and composes almost all the layers identified in this study. It groups all the porphyritic particles and associated loose minerals which have been provided by a single volcanic source. The second signature is marked by the presence of clastic components with a fluidal banded texture wrapping phenocrystals of plagioclase (Figs. 2, 4H, 9G and 11D). This signature is predominant in the deposits of Facies A in Tar channel system A, as well as in a layer of Facies G in Sámsonháza lobe axis and is present as secondary signature in a layer of Facies E in Sámsonháza lobe axis. Its specific position in the sedimentary sequence stratigraphically confirms the active role of channel A in feeding the lobe axis of Sámsonháza. The third signature is ephemeral, generally diluted by the first signature, and is marked by the presence of the putative obsidian particles found in two layers of Sámsonháza (Figs. 2, 8H and 10G). Similar coeval rocks, described as rhyolite extrusions, are documented in the Mátra Volcanic Complex (Káratson et al., 2001 and ref. therein). It is difficult to say why signature three has never been encountered in the proximal area of the NAF apron. The most likely way to transport such obsidian particles might have been by thin ash plumes which bypassed the Tar area and accumulated the detritus in the Sámsonháza area, being subsequently mixed with the preponderant submarine sedimentation of signature one. The absence of other kind of detritus, either volcanic or not, indicates that the apron was fed only by PDCs and ash plumes produced and immediately transferred to the basin by an island volcano or, less probable, a littoral volcano.

The rapid and unique accumulation of Facies A and related detritus intercalated in the volcano-sedimentary sequence could be interpreted as the result of the temporal growth and rapid collapse of a small dome on the flank of such volcano during a single eruptive period, similarly to what has been recently observed on the Kadovar Volcano (Plank et al., 2019). This event could be also taken as a marker level for further discussions on the evolution of the sedimentary system. The occurrence of Facies A at the base of channel system A, together with the occurrence of its peculiar detrital signature in the medial and upper part of the Sámsonháza sequence at SA could indicate that channel system A fed the upper part of the

Sámsonháza sequence SA, whereas the channel system B fed the lower part. This would suggest that channel system A was activated after channel sequence B, but further geochronological constrains are needed to validate this hypothesis.

7.2 Importance of the correct interpretation of volcanogenic sequences on basin scale

As shown by many authors, explosive eruptions change their physical behavior when interact with water, resulting in the accumulation of sequences with peculiar stratigraphic and petrographic characteristics (e.g., Trofimovs et al., 2008; Cuitiño and Scasso, 2013; Jutzeler et al., 2014; Di Capua and Groppelli, 2016a, b; Duraiswami et al., 2019). Such eruptions also deliver large amounts of detritus forcing the accumulation of sediments even where other factors (e.g., climate, tectonics) inhibit it (Di Capua and Scasso, 2020). Therefore, combining a good interpretation of mechanisms driving the accumulation of volcanogenic sequences with the possibility to gain precise geochronological constrains from them reveals the potential role that volcanogenic sequences could have in enabling the better resolution of sequence-stratigraphic tasks. The stratigraphic record of Tar and Sámsonháza offers a good example in this sense.

The accumulation of the TDF eruptive events (~14.9 Ma - Lukács et al., 2018) is temporal equivalent to the beginning of the Early Badenian transgressive phase in the Central Paratethys, that set up in the North Croatian Basin at ca. 15.35 (Brlek et al., 2020) and reached the Pannonian basin system around 15.1 Ma (e.g., Sant et al., 2017, 2019; Kováč et al., 2018; Vlček et al., 2020). In the study area, high sedimentation rates controlled by these multiple eruptive events initially contrasted the sea-level rise. This locally delayed the onset of the transgression, inducing the progradation of thick volcanogenic sequences that rapidly infilled the shallow-marine basins (Karátson et al., 2001). Such progradation ceased around 14.9 Ma, when the TDF sedimentation rates drastically decreased, and sea-level started to shift landward. During this shift, waters excavated a ravinement surface (erosional surface at the base of Log 11 - Fig. 2) associated with transgressive lag deposits corresponding to the subaqueous rhyodacite layers (Logs 1 and 11 - Fig. 2). The rhyodacitic submarine mudstones and siltstones documented in the Mátra Volcanic Complex (Karátson et al., 2001) own the same significance. Soon after, the onset of an andesite volcanism started to accumulate the NAF. The ravinement surface is absent in Sámsonháza because this is the distal part of the depocenter that was never exposed during the previous regression stage (Hámor, 1985).

In the Nógrád basin, voluminous amounts of NAF volcanogenic detritus were organized in the submarine apron during the transgression phase, as confirmed by the recovery of the bed of PLM intercalated in the NAF. In contrast, in the Mátra Volcanic Complex the volcanic morphologies and related deposits of the NAF were often accumulated subaerially (Karátson et al., 2001 and ref. therein). This difference indicates that the sea-level rise alone was again not able to contrast the volcanogenic sedimentation rates, therefore the increase in accommodation space in the Nógrád basin resulted from the combination of sea-level rise and strong subsidence rates (e.g., Vlček et al., 2020) driven by the activity of Zagyva Fault.

The sedimentary sequence of Sámsonháza gives constrains on what occurred from the onset of the NAF deposition during a transgressive phase until the end of the depositional cycle at ~ 14.4 Ma (Strauss et al., 2006; Kováč et al., 2018). Although geochronological ages are missing, it could be possible to speculate that the accumulation of the NAF ended further before the regression stage, because time was required to intrude and partially erode its sedimentary sequence. This would indicate that the NAF was accumulated in less than 400 ky, a time frame comparable to the mean lifespan of an eruptive centre similar to those of the Mátra Volcanic Complex (e.g., Price et al., 2012; Francalanci et al., 2013).

7.3 Volcanic control on the evolution of the volcanogenic apron evolution

The construction of submarine aprons proceeds through the aggradation of detritus during waxing-waning cycles that control the erosion and infill of channels and relative overbank deposits. These cycles have long been recognized in turbidite systems (e.g., Mutti and Normark, 1987, 1991), and their significance has been well described by McHargue et al. (2011 and ref. therein) as follows: during the waxing phase, dense and large flows tend to erode the channel conduit, which is then filled up during the waning phase by smaller flows. In classical turbidite systems, this cyclicity is controlled by allogenic processes (eustasy, climate and/or tectonics) (e.g., Catuneanu et al., 2011; Henstra et al., 2016) with a still unknown impact of one relative to another (McHargue et al., 2011).

In the proximal area of the NAF, each channel sequence, composed of the superimposition of FA2 onto FA1, corresponds to a sedimentation cycle, whose accumulation was controlled by volcanism, acting as the only allogenic process (Fig., 17A). In this case, the recognition of eruptive processes and their products, as well as their grouping into different Facies Associations on the base of their sedimentological and volcanological significance, allow to correlate the sedimentation cyclicity with the style of eruption that drove it. Waxing sedimentation phases occur when catastrophic and/or sustained eruptions produce flows alike to the high energetic flows of McHargue et al. (2011), which excavate scours/channels and accumulate thick, chaotic sequences of Facies A, B and C. Similar processes are very common around volcanic islands and generate scours and channels through which volcanogenic sediments are then easily transferred from the volcano to the basin (e.g., Casalbore et al., 2010, 2015; Watt et al., 2020). Waning sedimentation phases occur when minor eruptions produce flows alike to the low energetic flows of McHargue et al. (2011), which fill channels and accumulate overbank deposits rather than erode new paths. According to this model, each channel sequence and the correlated waxing-waning sedimentation cycle is a waxing-waning cycle of the volcanic activity.

Channels are then grouped into two different channel systems (Fig. 16), whose sedimentary record opens with deposits of highly destructive events, and upward continues with deposits of eruptions that drove the construction/reconstruction of the volcanic edifice. This trend individuates a second type of cyclicity of a hierarchical rank higher than the first one, which can be correlated to main stages of construction of the volcanic edifice (Fig. 17B). During these stages, eruptive style and frequency, as well as the eruptive centre position are almost constant (Martí et al., 2018). This causes the progressive definition of a sediment pathway and the construction of a channel system that progrades through time. Once major destructive events (e.g., sector collapse, caldera collapse) induce major modifications in the dynamics of the volcanic system, the eruptive centre position changes, promoting the shift of the sediment pathway and the formation of a new channel system. A modern example of such control is the Stromboli Island, where the progressive migration of the eruptive vents through time was accompanied by the generation of sector collapses which strongly influenced the development of the submarine aprons (Casalbore et al., 2010; Francalanci et al., 2013). Such modifications can also induce the periodic drawn of the volcanic edifice (e.g. Krakatau – Zen, 1970), locally controlling the frequency of the variation between sea level changes and sedimentary source: the faster the volcano edifice raises above the water, the more subaerially generated pyroclastic deposits will be accumulated into the basin, and the more failure events will affect the volcanic construction, leaving it below or at the sea level, the more hydrovolcanic sequences will be accumulated into the basin.

7.4 Interaction among volcanic processes, climate and seafloor morphology in distal areas

Apron distal offshoots are the place where the volcanic control on sediment accumulation is progressively dampened by other sedimentary processes, such as terrigenous sedimentation or biogenic accumulation of carbonate sequences (e.g., Bischoff et al., 2019). At the same time, seafloor topography strengthens its effects on the development of the sedimentary architectures (e.g., Prélat et al., 2009; Marini et al., 2015;

Soutter et al., 2019). The sedimentary succession of the NAF in Sámsonháza recorded both influences, testified by intercalation of PLM beds from one side, progressive facies transitions on the other side.

According to Randazzo et al. (1999), the accumulation of limestone beds in the Sámsonháza area occurred when the large amounts of sediments supplied by the syn-sedimentary volcanism temporally ceased and carbonate platforms were able to prograde. Volcanogenic detritus, like terrigenous detritus in mixed siliciclastic-carbonate sedimentary systems (e.g., Catuneanu et al., 2011), used to alter the environmental conditions at which submarine organisms live, preventing the accumulation of carbonate material. This mechanism controlled the alternation of limestone and volcanogenic beds in the basin, and it could be possible to speculate that limestone / volcanogenic beds' ratio is a function of the frequency of volcanic eruptions: the more frequent the volcanic eruptions are, the slower progradation characterizes the limestone sequences, as observed in the studied area.

On the other hand, seafloor topography controlled how the apron offshoots developed through space and time. Volcanogenic inputs were first funnelled into the ZT, where lobes began to prograde (base of Log 16). When sedimentation rates overcame accommodation rate into the trough, sediments started to spill over, and lobe started to shift. This shifting is testified by the superimposition of Facies Association 5 (lobe axis) onto Facies Association 4 (off-axis to fringe) in the ZT, and the coeval appearance of lobe fringe and off-axis deposits onto the ZR.

8. Conclusions

Improving the prediction on the distribution of volcanogenic sequences in the sedimentary records means to identify and comprehend the volcanic dynamics leading to the emplacement of different types of volcanogenic beds and the evolution of sedimentary architectures (e.g., Allen et al., 2007; Manville et al., 2009; Di Capua and Groppelli, 2018; Bischoff et al., 2019). In this view, this work studied the volcanogenic sequence of the NAF with a multiscale approach, unravelling how volcanic dynamics control the development of the sedimentary architecture of a submarine apron. The main results are below resumed.

1) The volcanogenic apron was constructed by the accumulation of volcanogenic detritus supplied by PDCs whose genesis and emplacement mechanisms strongly controlled their stratigraphic and petrographic features.
2) Petrographic analyses reveal that all the eruptive events were generated by the same source. Minor volcaniclastic detritus derived from older volcanogenic sequences and/or other coeval volcanic centres was taken in charge during the underwater motion of the flows.
3) The correct interpretation of volcanogenic deposits and their emplacement mechanisms represents a fundamental tool in constraining paleoenvironments of sedimentary basins and, consequently, variations of sea level in places where sedimentation is limited.
4) In the proximal area of the apron, channel infill-abandonment cycles correspond to waxing-waning eruptive cycles, whereas changes in channel system position reflect changes in the sediment pathway operated by major changes in the volcanic dynamics during the construction of the edifice.
5) In the distal apron offshoots, large supply of volcanogenic detritus has a so high impact on the environments that can temporally inhibit the progradation of carbonate platforms. Consequently, the more frequent are the explosive eruptions, the slower is the progradation of carbonate platforms in the basin.
6) Sedimentation rates of volcanogenic sequences could be as high as to result in the overcoming of structural seafloor barrier and the progradation of sedimentary architectures in areas where normal clastic sedimentation is physically prevented.

Acknowledgments

This work has been supported by the Hungarian–Italian MTA-CNR bilateral research project from 2016–2019 and 2020-2022 (led by S. Harangi and G. Groppelli). The work was partly supported by the Hungarian National Research, Development and Innovation Fund (NKFIH) within the FK OTKA project (No. 131869, from the end of 2019). R. Lukács is supported by the Bolyai János Research Fellowship. An early version of the manuscript has been improved by the fruitful comments of N. Németh and M. Brlek.

References

Allen, S.R., Hayward, B.W., Mathews, E., 2007. A facies model for a submarine volcaniclastic apron: the Miocene Manukau Subgroup, New Zealand. GSA Bulletin 119, 725-742.

Balázs, A., Maţenco, L., Magyar, I., Horváth, F., Cloetingh, S., 2016. The link between tectonics and sedimentation in back-arc basins: New genetic constraints from the analysis of the Pannonian Basin. Tectonics 35/6, 1526-1559.

Bischoff, A., Nicol, A., Cole, J., Gravley, D., 2019. Stratigraphy of Architectural Elements of Buried Monogenetic Volcanic System. Open Geoscience 11, 581-616.

Branney, M.J., Kokelaar, P., 2002. Pyroclastic density currents and the sedimentation of ignimbrites. Geol. Soc. Lond. Mem. 27.

Brlek, M., Kutterolf, S., Gaynor, S., Kuiper, K., Belak, M., Brčić, V., Holcova, K., Wang, K.-L., Bakrač, K., Hajek-Tadesse, V., Mišur, Horvat, M., Šuica, S., Schaltegger, U., 2020. Miocene syn‑rift evolution of the North Croatian Basin (Carpathian–Pannonian Region): new constraints from Mts. Kalnik and Požeška gora volcaniclastic record with regional implications. International Journal of Earth Sciences 109, 2775-2800.

Cardona, S., Wood, L.j., Dugan, B., Jobe, Z., Strachan, L.J., 2020. Characterization of the Rapanui mass-transport deposit and the basal shear zone: Mount Messenger Formation, Taranaki Basin, New Zealand. Sedimentology 67, 2111-2148.

Carey SN, Schneider J-L (2011) Volcaniclastic processes and deposits in the deep-sea. In: Hüneke H, Mulder T (eds) Deep-seasediments. Developments in sedimentology. Elsevier, Amsterdam, pp 457–51563

Casalbore, D., Romagnoli, C., Chiocci, F., Frezza, V., 2010. Morpho-sedimentary characteristics of the volcaniclastic apron around Stromboli volcano (Italy). Marine Geology 269, 132-148.

Casalbore, D., Bosman, A., Romagnoli, C., Chiocci, F.L., 2015. Morphology of Salina offshore (Southern Tyrrhenian Sea). Journal of Maps. DOI: 10.1080/17445647.2015.1070300

Catuneanu, O., Galloway, W.E., Kendall, C.G.St.C., Miall, A.D., Posamentier, H.W., Strasser, A., Tucker, M.E., 2011. Sequence Stratigraphy: Methodology and Nomenclature. Newsletters on Stratigraphy 44/3, 173-245.

Covault, J.A., Sylvester, Z., Hubbard, S.M., Jobe, Z.R., Sech, R.P., 2016. The stratigraphic record of submarine-channel evolution. The Sedimentary Record 14(3), 4-11.

Critelli, S., Ingersoll, R.V., 1995. Interpretation of neovolcanic versus paleovolcanic grains: an example from Miocene deep-marine sandstone of the Topanga Group (Southern California). Sedimentology 42, 783-804.

Csontos, L., Nagymarosy, A., Horváth, F., Kovác, M., 1992. Tertiary evolution of the intra-Carpathian area: a model. — Tectonophysics 208, 221-241.

Cuitiño, J.I., Scasso, R.A., 2013. Reworked pyroclastic beds in the early Miocene of Patagonia: Reaction in response to high sediment supply during explosive volcanic events. Sedimentary Geology 289, 194-209.

Cunha, R.S., Tinterri, R., Magalhaes, P.M., 2017. Annot Sandstone in Peïra Cava basin: An example of an asymmetric facies distribution in a confined turbidite system (SE France). Marine and Petroleum Geology 87, 60-79.

De Blasio, F.V., Elverhøi, A., 2011. Properties of Mass-Transport Deposits as inferred from dynamic modelling of subaqueous mass wasting: a short review. In: Shipp, R.C., Weimer, P., Posamentier, H.W. (Eds) Mass-transport deposits in deepwater settings. SEPM Special Publication, London.

Di Capua, A., Groppelli, G., 2016a. Application of actualistic models to unravel primary volcanic control on sedimentation (Taveyanne Sandstones, Oligocene Northalpine Foreland Basin). Sedimentary Geology 336, 147-160.

Di Capua, A., Groppelli, G., 2016b. Emplacement of pyroclastic density currents (PDCs) in a deep-sea environment: the Val d'Aveto Formation case (Northern Apennines, Italy). Journal of Volcanology and Geothermal Research 328, 1-8.

Di Capua, A., Groppelli, G., 2018. The riddle of volcaniclastic sedimentation in ancient deep-water basins: A discussion. Sedimentary Geology 378, 52-60.

Di Capua, A., Scasso, R.A., 2020. Sedimentological and petrographic evolution of a fluvio-lacustrine environment during the onset of volcanism: Volcanically-induced forcing of sedimentation and environmental responses. Sedimentology 67, 1879-1913.

Dodd, T.J.H., Leslie, A.G., Gillespie, M.R., Dobbs, M.R., Bide, T.P., Kendall, R.S., Kearsey, I., Chiam, K., Goay, M., 2020. Deep to shallow-marine sedimentology and impact of volcanism within the Middle Triassic Palaeo-Tethyan Semantan Basin, Singapore. Journal of Asian Earth Sciences 196.

Douillet, G.A., Bernard, B., Bouysson, M., Chaffaut, Q., Dingwell, D.B., Gegg, L., Hoelscher, I., Kueppers, U., Mato, C., Ritz, V.A., Schlunegger, F., Witting, P., 2018. Pyroclastic dune bedforms: macroscale structures and lateral variations. Examples from the 2006 pyroclastic currents at Tungurahua (Ecuador). Sedimentology 66, 1531-1559.

Douillet, G.A., Pacheco, D.A., Kueppers, U., Letort, J., Tsang-Hin-Sun, È., Bustillos, J., Hall,M., Ramòn, P., Dingwell, D.B., 2013. Dune bedforms produced by dilute pyroclastic density currents from the August 2006 eruption of Tungurauha volcano, Ecuador. Bulletin of Volcanology 75, 1–20.

Douillet, G.A., Taisne, B., Tsang-Hin-Sun, È.,Müller, S.K., Kueppers, U., Dingwell, D.B., 2015. Syn-eruptive, soft-sediment deformation of deposits from dilute pyroclastic density currents: triggers from granular shear, dynamic pore pressure, ballistic impacts and shock waves. Solid Earth 6, 553–572.

Downes, H., Pantó, G., Póka, T., Mattey, D.P., Greenwood, P. B., 1995. Calc-alkaline volcanics of the Inner Carpathian arc, Northern Hungary: new geochemical and oxygen isotopic results. — In: H. Downes & O. Vaselli (szerk.): Neogene and related volcanism in the Carpatho-Pannonian Region. Acta Volcanologica, pp. 29-41.

Dunham, R.J., 1962. Classification of carbonate rocks according to depositional texture. In: Classification of Carbonate Rocks (Ed. E.D. Ham), American Association of Petroleum Geologists Memoir, 1, 108–121.

Duraiswami, R.A., Jutzeler, M., Karve, A.V., Gadpallu, P., Kale, M.G., 2019. Subaqueous effusive and explosive phases of late Deccan volcanism: evidence from Mumbai Islands, India. Arabian Journal of Geosciences 12, pp.21.

Etienne, S., Mulder, T., Bez, M., Desaubliaux, G., Kwaniewski, A., Parize, O., Dujoncquoy, E., Salles, T., 2012. Multiple scale characterization of sand-rich distal lobe deposit variability: Examples from the Annot Sandstones Formation, Eocene–Oligocene, SE France. Sedimentary Geology 273-274, 1-18.

Fauria, K.E., Manga, M., Wei, Z., 2017. Trapped bubbles keep pumice afloat and gas diffusion makes pumice sink. Earth and Planetary Science Letters 460, 50-59.

Fodor, L., Csontos, L., Bada, G., Györfi, I. & Benkovics, L. 1999: Tertiary tectonic evolution of the Pannonian basin system and neighbouring orogens: a new synthesis of palaeostress data. - in Durand, B., Jolivet, L., Horváth F. és Séranne, M. (Szerk.), The Mediterranean Basins: Tertiary Extension within the Alpine Orogen. — Geological Society, London, Special Publications 156, 295-334.

Francalanci, L., Lucchi, F., Keller, J., De Astis, G., Tranne, C.A., 2013. Eruptive, volcano-tectonic and magmatic history of the Stromboli volcano (north-eastern Aeolian archipelago). In: Lucchi, F., Peccerillo, A., Keller, J., Tranne, C.A., Rossi, P.L. (Eds): The Aeolian Islands Volcanoes. Geological Society, London, Memoirs, 37, London.

Gyalog L. (Ed) 2005 Explanatory for Geological Map of Hungary 1:100 000 Hung. Geol. Inst. p. 1-189.

Hámor, G., 1985. Geology of the Nógrád-Cserhát area. Geologica Hungarica, Ser. Geol. 22, 234 p.

Harangi, S. & Lenkey, L., 2007. Genesis of the Neogene to Quaternary volcanism in the Carpathian-Pannonian region: Role of subduction, extension, and mantle plume. Geological Society of America Special Papers 418, 67-92.

Harangi, S., 2001. Neogene to Quaternary Volcanism of the Carpathian-Pannonian Region - a review. Acta Geologica Hungarica 44, 223-258.

Harangi, S., Downes, H., Kósa, L., Szabó, C., Thirlwall, M. F., Mason, P.R.D., Mattey, D., 2001. Almandine garnet in calc-alkaline volcanic rocks of the Northern Pannonian Basin (Eastern-Central Europe): geochemistry, petrogenesis and geodynamic implications. Journal of Petrology 42/10, 1813-1843.

Harangi, S., Downes, H., Thirlwall, M. & Gméling, K., 2007. Geochemistry, petrogenesis and geodynamic relationships of Miocene calc-alkaline volcanic rocks is the Western Carpathian Arc, eastern central Europe. Journal of Petrology 48, 2261-2287.

Henstra, G.A., Grundvåg, G.A., Johannessen, E.P., Kristensen, T.B., Midtkandal, I., Nystuen, J.P., Rotevatn, A., Surlyk, F., Sæther, T., Windelstad, J., 2016. Depositional processes and stratigraphic architecture within a coarse-grained rift-margin turbidite system: The Wollaston Foreland Group, east Greenland. Marine and Petroleum Geology 76, 187-209.

Horváth, F., Musitz, B., Balázs, A., Végh, A., Uhrin, A., Nádor, A., Koroknai, B., Pap, N., Tóth, T., Wórum, G., 2015. Evolution of the Pannonian basin and its geothermal resources. Geothermics 53, 328-352.

Jobe, Z.R., Howes, N.C., Auchter, N.C., 2016. Comparing submarine and fluvial channel kinematics: Implications for stratigraphic architecture. Geology 44, 931-934.

Jutzeler, M., Manga, M., White, J.D.L., Talling, P.J., Proussevitch, A.A., Watt, S.F.L., Cassidy, M., Taylor, R.N., Le Friant, A., Ishizuka, O., 2016. Submarine deposits from pumiceous pyroclastic density currents traveling over water: An outstanding example from offshore Montserrat (IODP 340). GSA Bulletin 129, 392-414.

Jutzeler, M., McPhie, J., Allen, S.R., 2014. Facies architecture of a continental, below-wave-base volcaniclastic basin: The Ohanapecosh Formation, Ancestral Cascades arc (Washington, USA). GSA Bulletin 126, 352-376.

Kane, I.A., Pontén, A.S.M., 2012. Submarine transitional fl ow deposits in the Paleogene Gulf of Mexico. Geology 40, 1119-1122.

Karátson, D., Csontos, L., Harangi, S., Székely, B., Kovácsvölgyi, S., 2001. Volcanic successions and the role of destructional events in the Western Mátra Mountains, Hungary: implications for the volcanic structures. GeomorpGéomorphologie: relief, processus, environnement 7, 79 – 92.

Kováč, M., Halásová, E., Hudáčková, N., Holcová, K., Hyžný, M., Jamrich, M., Ruman, A., 2018. Towards better correlation of the Central Paratethyds regional time scale with the standard geological time scale of the Miocene Epoch. Geologica Carpathica 69, 283-300.

Li, P., Kneller, B.C., Hansen, L., Kane, I.A., 2016. The classical turbidite outcrop at San Clemente, California revisited: an example of sandy submarine channels with asymmetric facies architecture. Sedimentary Geology 346, 1-16.

Lukács, R., Harangi, S., Bachmann, O., Guillong, M., Danišík, M., Buret, Y., Von Quadt, A., Dunkl, I., Fodor, L., Sliwinski, J., Soós, I., Szepesi, J., 2015. Zircon geochronology and geochemistry to constrain the youngest eruption events and magma evolution of the Mid-Miocene ignimbrite flare-up in the Pannonian Basin, eastern central Europe. — Contributions to Mineralogy and Petrology 170/5, 52.

Lukács, R., Harangi, S., Guillong, M., Bachmann, O., Fodor, L., Buret, Y., Dunkl, I., Sliwinski, J., Von Quadt, A., Peytcheva, I. & Zimmerer, M., 2018. Early to Mid-Miocene syn-extensional massive silicic volcanism in the Pannonian Basin (East-Central Europe): Eruption chronology, correlation potential and geodynamic implications. Earth-Science Reviews 179, 1-19.

Magyar, I., Geary, D.H., Müller, P., 1999. Paleogeographic evolution of the Late Miocene Lake Pannon in Central Europe. Palaeogeography, Palaeoclimatology, Palaeoecology 147, 151-167.

Manville, V., Németh, K., Kano, K., 2009. Source to sink: A review of three decades of progress in the understanding of volcaniclastic processes, deposits, and hazards. Sedimentary Geology 220, 136-161.

Marini, M., Milli, S., Ravnås, R., Moscatelli, M., 2015. A comparative study of confined vs. semiconfined turbidite lobes from the Lower Messinian Laga Basin (Central Apennines, Italy): Implications for assessment of reservoir architecture. Marine and Petroleum Geology 63, 142-165.

Martì, J., Groppelli, G., da Silveira, A.B., 2018. Volcanic stratigraphy: a review. Journal of Volcanology and Geothermal Research 357, 68-91.

McHargue, T., Pyrcz, M.J., Sullivan, M.D., Clark, J.D., Fildani, A., Romans, B.W., Covault, J.A., Levy, M., Posamentier, H.W., Drinkwater, N.J., 2011. Architecture of turbidite channel systems on the continental slope: Patterns and predictions. Marine and Petroleum Geology 28, 728-743.

McPhie, J., Doyle, M., Allen, R., 1993. Volcanic Textures: a guide to the interpretation of textures in volcanic rocks. CODES Key Centre, University of Tasmania, Hobart.

Mulder, T., Alexander, J., 2001. The physical character of subaqueous sedimentary density flows and their deposits. Sedimentology 48, 269–299.

Mutti, E., Bernoulli, D., Ricci Lucchi, F., Tinterri, R., 2009. Turbidites and turbidity currents from Alpine “flysch” to the exploration of continental margins. Sedimentology 56, 267-318.

Mutti, E., Normark, W.R., 1987. Comparing examples of modern and ancient turbidite systems: problems and concepts. In: Marine Clastic Sedimentology (Eds J.K. Legget and G.G. Zuffa), pp. 1–38, Graham and Trotman, London.

Mutti, E., Normark, W.R., 1991. An integrated approach to the study of turbidite systems. In P. Weimer, & H. Link (Eds.), Seismic facies and sedimentary processes of submarine fans and tudbidite systems, Ann Arbore. New York, Springer. Pp. 75-106.

Mutti, E., Tinterri, R., Benevelli, G., di Biase, G., Cavanna, G., 2003. Deltaic, mixed and turbidite sedimentation in ancient foreland basins. Marine and Petroleum Geology 20, 733-755.

Nagymarosy, A., Hámor, G., 2013. Genesis and Evolution of the Pannonian Basin. In: J. Haas (Ed), Geology of Hungary, Regional Geology Reviews, Springer-Verlag Berlin Heidelberg.

Pécskay, Z., Lexa, J., Szakács, A., Seghedi, I., Balogh, K., Konečny, V., Zelenka, T., Kovács, M., Póka, T., Fulop, A., Márton, E., Panaiotu, C., Cvetkovic, V., 2006. Geochronology of Neogene magmatism in the Carpathian arc and intra-Carpathian area. Geologica Carpathica 57/6, 511-530.

Pelikán, P., Rónai, A., (Eds.) 2005. Geological map of Hungary. 1:100 000. L-34-4. Gyöngyös Hung. Geol. Inst.

Pierce, C.S., Haughton, P.D.W., Shannon, P.M., Pulham, A.J., Barker, S.P., Martinsen, O.J., 2018. Variable character and diverse origin of hybrid event beds in a sandy submarine fan system, Pennsylvanian Ross Sandstone Formation, western Ireland. Sedimentology 65, 952-992.

Plank, S., Walter, T.R., Martinis, S., Cesca, S., 2019. Growth and collapse of a littoral lava dome during the 2018/19eruption of Kadovar Volcano, Papua New Guinea, analyzed bymulti-sensor satellite imagery. Journal of Volcanology and Geothermal Research 388, pp.15.

Póka, T., Seghedi, I., Márton, E., Zelenka, T., Pécskay, Z., 2004. Miocene volcanism of the Cserhát Mts (N Hungary): Integrated volcano-tectonic, geochronologic and petrochemical study. Acta Geologica Hungarica 47(2-3), 221-246.

Prakfalvi, P. (Ed) 2005. Geological map of Hungary. 1:100 000. M-34-136 Salgótarján Hung. Geol. Inst.

Prélat, A., Hodgson, D., 2013. The full range of turbidite bed thickness patterns in submarine lobes: controls and implications. The Journal of the Geological Society 170, 209-214.

Prélat, A., Hodgson, D.M., Flint, S.S., 2009. Evolution, architecture and hierarchy of distributary deep-water deposits: a high-resolution outcrop investigation from the Permian Karoo Basin, South Africa. Sedimentology 56, 2132-2154.

Price, R.C., Gamble, J.A., Smith, I.E.M., Maas, R., Waight, T., Stewart, R.B., Woodhead, J., 2012. The Anatomy of an Andesite Volcano: a Time-Stratigraphic Study of Andesite Petrogenesis and Crustal Evolution at RuapehuVolcano, New Zealand. Journal of Petrology 53, 2139-2189.

Püspöki, Z., Hámor-Vidó, M., Pummer, T., Sári, K., Lendvay, P., Selmeczi, I., Detzky, G., Gúthy, T., Kiss, J., Kovács, Zs., Prakfalvi, P. McIntohs, R.W., Buday-Bódi, E., Báldi, K., Markos, G., 2017. A sequence stratigraphic investigation of a Miocene formation supported by coal seam quality parameters – Central Paratethyds, N-Hungary. International Journal of Coal Geology 179, 196-210.

Randazzo, A.F., Müller, P., Lelkes, G., Juhász, E., Hámor, T., 1999. Cool-water limestones of the Pannonian basinal system, Middle Miocene, Hungary. Journal of Sedimentary Research 69, 283-293.

Rögl, F., 1999. Mediterranean and Paratethys. Facts and hypotheses of an Oligocene to Miocene paleogeography (short overview). Geologica Carpathica 50, 339-349.

Roverato, M., Larrea, P., Casado, I., Mulas, M., Béjar, G., Bowman, L., 2018. Characterization of the Cubilche debris avalanche deposit, a controversial case from the northern Andes, Ecuador. Journal of Volcanology and Geothermal Research 360, 22-35.

Royden, L. H., Horváth, F., Burchfiel, B. C., 1982. Transform faulting, extension, and subduction in the Carpathian Pannonian region. GSA Bulletin 93/8, 717-725.

Royden, L., Horváth, F., Rumpler, J., 1983. Evolution of the Pannonian Basin System: 1. Tectonics. Tectonics 2/1, 63-90.

Sant K, Palcu D, Mandic O, Krijgsman W (2017) Changing seas in the Early-Middle Miocene of Central Europe: a Mediterranean approach to Paratethyan stratigraphy. Terra Nova 29, 273–281.

Sant K, Palcu DV, Turco E, Di Stefano A, Baldassini N, Kouwenhoven T, Kuiper KF, Krijgsman W (2019) The mid-Langhian flooding in the eastern Central Paratethys: integrated stratigraphic data from the Transylvanian Basin and SE Carpathian Foredeep. J. Earth Sci 108, 2209–2232.

Schindlbeck JC, Kutterolf S, Freundt A, Scudder RP, Pickering KT, Murray RW (2013) Emplacement processes of submarine volcaniclastic deposits (IODP Site C0011, Nankai Trough). Mar Geol 343, 115–124.

Schwarzkopf, L.M., Schmincke, H.-U., Cronin, S.J., 2005. A conceptual model for block-and-ash flow basal avalanche transport and deposition, based on deposit architecture of 1998 and 1994 Merapi flows. Journal of Volcanology and Geothermal Research 139, 117-134.

Seghedi, I. & Downes, H., 2011. Geochemistry and tectonic development of Cenozoic magmatism in the Carpathian–Pannonian region. Gondwana Research 20/4, 655-672.

Seghedi, I., Downes, H., Harangi, S., Mason, P. R. D. & Pécskay, Z., 2005. Geochemical response of magmas to Neogene–Quaternary continental collision in the Carpathian–Pannonian region: A review. Tectonophysics 410/1, 485-499.

Seghedi, I., Downes, H., Szakács, A., Mason, P. R. D., Thirlwall, M. F., Roşu, E., Pécskay, Z., Márton, E. & Panaiotu, C., 2004. Neogene–Quaternary magmatism and geodynamics in the Carpathian–Pannonian region: a synthesis. Lithos 72/3, 117-146.

Shanmugam, G., Moiola, R.J., 1988. Submarine Fans: Characteristics, Models, Classification, and Reservoir Potential. Earth-Science Reviews 24, 383-428.

Shumaker, L.E., Sharman, G.R., King, P.R., Graham, S.A., 2018. The source is in the sink: deep-water deposition by a submarine volcanic arc, Taranaki Basin, New Zealand. Sedimentology 65, 2506-2530.

Sinclair, H., & Tomasso, M., 2002. Depositional evolution of confined turbidite basins. Journal of Sedimentary Research 72, 451-456.

Smith, G.A., 1991. Facies sequences and geometries in continental volcaniclastic sediments. In: Fisher, R.V., Smith, G.A. (Eds.), Sedimentation in Volcanic Settings. SEMP Special Publication 5, pp. 109–121.

Sohn, Y.K., Park, K.H., Yoon, S.-H., 2008. Primary versus secondary and subaerial versus submarine hydrovolcanic deposits in the subsurface of Jeju Island, Korea. Sedimentology 55, 899-924.

Soutter, E.L., Kane, I.A., Fuhrmann, A., Cumberpatch, Z.A., Huuse, M., 2019. The stratigraphic evolution of onlap in siliciclastic deep-water systems: autogenic modulation of allogenic signals. Journal of Sedimentary Research 89, 890-917.

Strauss, P., Harzhauser, M., Hinsch, R., Wagreich, M., 2006. Sequence stratigraphy in a classic pull-apart basin (Neogene, Vienna Basin). A 3D seismic based integrated approach. Geologica Carpathica 57, 185-197.

Sulpizio, R., Dellino, P., Doronzo, D.M., Sarocchi, D., 2014. Pyroclastic density currents: state of the art and perspectives. Journal of Volcanology and Geothermal Research 283, 36–65.

Szabó, C., Harangi, S. & Csontos, L., 1992, Review of Neogene and Quaternary volcanism of the Carpathian-Pannonian region. Tectonophysics 208/1, 243-256.

Szepesi, J., Lukács, R., Soós, I., Benkó, Z., Pécskay, Z., Ésik, Z., Kozák, M., Di Capua, A., Groppelli, G., Norini, G., Sulpizio, R., Harangi, S., 2019. Telkibánya lava domes: lithofacies architecture of a Miocene rhyolite field (Tokaj Mountains, Carpathian-Pannonian region, Hungary). Journal of Volcanology and Geothermal Research 385, 179-197.

Tari, G., Dövényi, P., Horváth, F., Dunkl, I., Lenkey, L., Stefanescu, M., Szafián, P. & Tóth, T. 1999: Lithospheric structure of the Pannonian Basin derived from seismic, gravity and geothermal data. In: B. Durand, L. Jolivet, F. Horváth & S. M. (szerk.): The Mediterranean Basins: Tertiary extension within the Alpine orogen. Geological Society, London, Special Publication, pp. 215-250.

Tari, G., Horváth, F. & Rumpler, J. 1992: Styles of extension in the Pannonian Basin. — Tectonophysics 208/1, 203-219.

Trofimovs, J., Cas, R.A.F., Davis, B.K., 2004. An Archean submarine volcanic debris avalanche deposit, Yilgarn Craton, western Australia, with komatiite, basalt and dacite megablocks. The product of a dome collapse. Journal of Volcanology and Geothermal Research 138, 111-126.

Trofimovs, J., Sparks, R.S.J., Talling, P.J., 2008. Anatomy of a submarine pyroclastic flow and associated turbidity current: July 2003 dome collapse, Soufrière Hills volcano, Montserrat, West Indies. Sedimentology 55, 617-634.

Ui, T., Kawachi, S., Neall, V.E., 1986. Fragmentation of debris avalanche material during flowage – Evidence from the Pungarehu Formation, Mount Egmont, New Zealand. Journal of Volcanology and Geothermal Research 27, 255-264.

Vakarcs, G., Hardenbol, J., Abreu, V.S., Vail, P.R., Várnai, P., Tari, G., 1998. Oligocene – Middle Miocene depositional sequences of the Central Paratethyds and their correlation with regional stages. In: Mesozoic and Cenozoic Sequence Stratigraphy of European Basins, SEPM Special Publication n.60, London.

Vlček, T., Šarinová, K., Rybár, S., Hudáčková, N., Jamrich, M., Šujan, M., Franců, J., Nováková, P., Sliva, L., Kováč, M., Kováčová, M., 2020. Paleoenvironmental evolution of Central Paratethys Sea and Lake Pannon during the Cenozoic. Palaeogeography, Palaeoclimatology, Palaeoecology 559, pp.17.

Wadsworth, F.B., Vasseur, J., von Aulock, F.W., Hess, K.-U., Scheu, B., Lavallé, Y., Dingwell, D.B., 2014. Nonisothermal viscous sintering of volcanic ash. J. Geophys. Res. Solid Earth 119. http://dx.doi.org/10.1002/2014JB011453.

Watt, S.F.L., Karstens, J., Berndt, C., 2020. Volcanic-Island lateral collapses and their submarine deposits. In: Roverato, M., Dufresne, A., Procter, J. (Eds.): Volcanic Debris Avalanches: from collapse to hazard. Advances in Volcanology Series. Springer Nature Switzerland.

Závada, P., Kratinová, Z., Kusbach, V., Schulmann, K., 2009. Internal fabric development in complex lava domes. Tectonophysics 466, 101-113.

Zen, M.T., 1970. Growth and State of Anak Krakatau in September 1968. Bulletin Volcanologique 34, 205-215.

Figure Captions

Figure 1: A) Geological sketch of the main tectono-magmatic structures of the Nógrád Basin and geological map of the study area modified from Pelikan and Ronai (2005), and Prakfalvi (2005). SzF = Szentkut Fault; SaF = Sámsonháza Fault; ZR = Zagyva Ridge; ZT = Zagyva Trough; ZF = Zagyva Fault; TA = Tar site A; TB = Tar site B; TC = Tar site C; SA = Sámsonháza site A; SB = Sámsonháza site B; SC = Sámsonháza site C; GBF = Garab Schlier Formation; FF = Fót Formation; HAF = Hasznos Andesite Formation; TDF = Tar Dacite Tuff Formation; NAF = Nagyhársas Andesite Formation; RLM = Rákos Limestone Member; ONF = other Neogene Formations younger than the Leithakalk Formation (FF in Fig. 1B) and not object of this work. B) General stratigraphy of the Nógrád Basin in the study area. Ep. = Epoch; RS = Regional Stages; Lithostrat. = Lithostratigraphy; GBF = Garab Schlier Formation; FF = Fót Formation; HAF = Hasznos Andesite Formation; TDF = Tar Dacite Tuff Formation; NAF = Nagyhársas Andesite Formation; LF = Leithakalk Formation, subdivided into PLM (Pécsszabolcs Limestone Member) and RLM (Rákos Limestone Member). Lithostratigraphy and biostratigraphy according to Vakarcs et al. (1998) and Gyalog (2005); stratigraphic position of TDF according to zircon ages of Lukács et al. (2018); stratigraphic positions of HAF and NAF according to Hámor (1985) and K/Ar ages of Póka et al. (2004). The upper boundary of HAF has no temporal constrains, but is older than TDF (Hámor, 1985; Póka et al., 2004). C) General logs compiled after fieldwork. GBF = Garáb Schlier Formation; FF = Fót Formation; HAF = Hasznos Andesite Formation; TDF = Tar Dacite Tuff Formation; NAF = Nagyhársas Andesite Formation; PLM = Pécsszabolcs Limestone Member; RLM = Rákos Limestone Member.

Figure 2: Logs measured in the field. Numbers are depicted in Fig. 1A. LF = Leithakalk Formation; X = presence of fluidal banded rock fragments described in Facies A; Y = presence of putative obsidian rock fragments (see the Results and Interpretation paragraph for further details). Crossed parts indicate beds not studied because covered by debris.

Figure 3: A) General view of the sequence exposed in the site SA of Sámsonháza. B) Fluidized contact between the lowermost andesite sill (bottom) and the NAF (top). C) Erosional contact between the uppermost andesite sill (bottom) and the RLF (top).

Figure 4: Main lithostratigraphic features of Facies A: A) basal ash unit overlain by normally graded breccia unit. Megablocks are frequently fractured (B), and cracks are filled by injected ashy matrix characterized by a sigmoidal lamination (C). D) Flattened and broken block. Main petrographic features of Facies A matrix: E) phenocrystals of plagioclase (white arrow) and irregular pumices (in white) in a highly vesiculated brown matrix. Note that vesicles are rimmed, and only ne is filed up by palagonitized glass (red arrow). F) Other components of Facies A: dark scoriaceous fragments with vesicles (red arrow) in a vesiculated groundmass. G) When not vesiculated, groundmass is very fine and glassy. Porphiritic rock fragments are also present (red arrow). H) Main petrographic features of blocks and megablocks, constituted by phenocrystals and laths of plagioclase embedded in a banded fluidal texture (white arrow). All the microphotographs were taken under parallel nichols.

Figure 5: Main lithostratigraphic features of Facies B: A) massive, poorly sorted tuff-breccia deposits, with angular to subangular intermediate lava blocks. Breccia deposits are generally matrix-supported (B) but locally become clast-supported (C). Main petrographic features of Facies B: lithics are the main components, and generally show a porphyritic texture with phenocrystals of plagioclase and pyroxene (D), or phenocrystals and cumulate of plagioclase (E), with a groundmass colour that varies from light grey, to yellow, dark red and brown (D-G). In minor amounts, loose crystals of plagioclase, pyroxene (H), rarely arranged in clots (I), are present. Matrix is generally glassy and weathered into a yellow mixture of phyllosilicate and palagonite (D and H – red arrows). Rarely, some components are rimmed by palagonite (I – red arrows). All the microphotographs were taken under parallel nichols.

Figure 6: Main lithostratigraphic features of Facies C: amalgamated, massive to weakly laminated thick deposits, where the juxtaposition of ash- to lapilli-size detritus is interrupted by blocks isolated or arranged in elongated pockets (A). Crossbedding to parallel laminations are frequently truncated (B-C). D) Nlock with

ball and pillow structures at the bottom. E) Coarse- to fine-grained beds overlain by a dune structure (white arrows). Main petrographic features of Facies C – petrofacies C1: F) rounded intermediate lithics rimmed by palagonitized glass (red arrows), juxtaposed one to each other (microphotograph under parallel nichols). Note that palagonite also substitutes intragranular glass (black arrows). G) Microcrystalline groundmass developed where particles are not in contact (black arrow). The bottom of the microphotograph is under paraller nichols, whereas the top is under crossed nichols.

Figure 7: Main petrographic features of Facies C – petrofacies C1: A) Rimmed vesiculated groundmass, hosting irregular yellow scoriae (B – in white). C) Pyroxene clot with a palagonitized glassy core (red arrow). D) Lathworks in a dark, glassy and weathered groundmass. E and F) Ameboid porphyritic lithics with phenocrystals and laths of plagioclase, embedding the partially palagonitized groundmass of the deposit (red arrows). When groundmass is vitric and vesiculated, palagonite substitutes the vitric components but preserves the groundmass structures (G and H – red arrows). Main petrographic features of Facies C – petrofacies C2: I) rhyolitic fragments characterized by a high vesiculation and fluidal texture, rarely wrapping phenocrystals of quartz and biotite, embedded in a glassy matrix devitrified into clay (black arrows). J) Plugs of well sorted particles, mainly composed of loose crystals of quartz, plagioclase, sanidine and biotite, occasionally populate the samples, or (K) are arranged forming gas pipe-like structures (black arrow). All the microphotographs were taken under parallel nichols.

Figure 8: Main lithostratigraphic features of Facies D: massive lapilli-tuff (A) and tuff (B) deposits of Facies D. Main petrographic features of Facies D: ameboid or irregular intermediate scoria fragments, irregular to rounded lava fragments and minor loose crystals of plagioclase, rimmed by a thin vitric boundary (white arrows C – E). Groundmass is often vesiculated, and vesicles are characterized by a vitric rim (red arrows - F and G) or filled up by palagonitized glass (black arrows - C and D). H) Microphotograph of an obsidian fragment documented in Sámsonháza samples. All the microphotographs were taken under parallel nichols.

Figure 9: Main lithostratigraphic features of Facies E: A) Reverse-to-normal graded deposits, with a basal part overlain by a coarser lapilli-size unit and an upper wavy fine-grained part. Main petrographic features of Facies E: glassy to vesiculated matrix (B – white arrow), embedding loose crystals of plagioclase, occasionally vesiculated (black arrows – C), and scoriaceous, dark brown lava fragments (black arrows - D). Microphotographs were taken under parallel nichols. Groundmass is occasionally microcrystalline (E – bottom under crossed nichols, top under parallel nichols) and vesicles could be rimmed (black arrows - F) (under parallel nichols). Fragments of lava, with petrographic features similar to those described in Fig. 2H, are highly vesiculated and rimmed by palagonite (white arrows - G) (under parallel nichols).

Figure 10: Normally graded deposits of Facies F (A). Main petrographic features of Facies F – petrofacies F1: large amount of intermediate ameboid, irregular and subrounded porphyritic lava fragments (B and C) in a brown devitrified groundmass (white arrows - B and C). All microphotographs were taken under parallel nichols. D) Large pumice including loose phenocrystals of zoned plagioclase and pyroxene (C – bottom under crossed nichols, top under parallel nichols). E) Loose crystals of plagioclase, pumices (white arrows) and related fragments (red arrow). Microphotograph was taken under parallel nichols. F) Flattered pumices in a dark brown groundmass, as arranged in a sample of Sámsonháza. Microphotograph was taken under parallel nichols. G) Obsidian-like fragments encountered in a Facies F layer of Sámsonháza. Microphotograph was taken under parallel nichols. Main petrographic features of Facies F – petrofacies F2: loose crystals of quartz, plagioclase, biotite and minor sanidine, fluidal fragments of rhyodacite (black arrows), rare fragments of intermediate lava (red arrows) (H) and shards (black arrows I). All microphotographs were taken under parallel nichols.

Figure 11: A) Well sorted, normally graded bed of Facies G with large angular pumices (white arrows) and mixed with finer, dark and angular scoriaceous detritus. Main petrographic features of Facies G: B) Large pumices and black scoriae with a good degree of palagonitization (red arrows). C) Large pumice with rimmed vesicles (red arrows). D) Lava fragment with petrography and texture alike to those of megablocks in Facies A are observed (*cfr* Fig. 4H). All microphotographs were taken under parallel nichols.

Figure 12: A) layer of Facies H in Tar (bordered in white). Main petrographic features of Facies H. B) Wavy laminated, well sorted layers composed of fine to very fine ash. Facies H is generally composed of loose crystals of plagioclase and pyroxene, dark intermediate fragments with rare phenocrystals of plagioclase and glassy fragments (C). Often, palagonite wraps particles (black arrows - D and E). F) A well sorted lamina of fine ash, where particles are cemented together by secondary palagonite (black arrows). All microphotographs were taken under parallel nichols.

Figure 13: marly limestone layer of Facies I (A), where bivalves (in the white circle - B) and gastropods (C) are included. Main petrographic features of Facies I: porphyritic lava fragment embedded in a carbonate matrix (microphotograph under crossed nichols - D). Note that some plagioclase phenocrystals have been substituted by secondary calcite (white arrow). E) Single minerals of quartz and plagioclase (white arrows) and a lava rock fragment (red arrow). Parallel nichols on the left, crossed nichols on the right. F) Gastropod fossil (parallel nichols). G) Porphyritic lava fragments almost entirely substituted by secondary calcite (crossed nichols).

Figure 14: Examples of Facies Associations in three key areas. A) Facies Association 1 (Facies C, Facies A, Facies C) overlain by Facies Association 2 in Log 2 (site TA of Tar). Red line corresponds to an erosive surface observed between Facies C and Facies A. B) Facies Association 2 (Facies D) erosively overlain by Facies Association 1 (Facies C) in Log 8 (site TB of Tar). Red line highlights the erosive contact. C) Facies Association 4 that upward evolves into Facies Association 5 in Logs 14 and 15 (site SA of Sámsonháza). Red arrow indicates a lateral pinch out typical of beds in Facies Association 4.

Figure 15: Reconstruction of the apron sub-environments through log correlations and facies association identification. LF = Leithakalk Formation.

Figure 16: Reconstruction of the volcanogenic apron on a basin scale. Lateral extension of the TDF is limited to the study area. T = Tar; S = Sámsonháza; TDF = Tar Dacite Tuff Formation; red dash line = Sámsonháza Fault; white lines are TA = Tar Site A; TB = Tar Site B; TC = Tar Site C; SA = Sámsonháza Site A; SB = Sámsonháza Site B; SC = Sámsonháza Site C. Green arrows indicate paleocurrents and paleochannel directions measured in the field. Colours refer to Fig. 15.

Figure 17: Volcanologically - controlled hierarchy in the construction of the proximal apron architectures. A) On a low hierarchical level, channel architectures are built up by the alternations among major and minor eruptive events. During major eruptive events, channels are deeply eroded, whereas during minor eruptive events they are filled up. B) On a higher hierarchical level, constructive phases during the growth of a volcanic edifice favours the generation of a stable sediment pathway which constantly fills a channel system. Destructive phases deeply change the morphology of a volcanic edifice and generally induce a major change in the sediment paths that supply the submarine aprons, forcing the abandonment of old channel systems for new ones.

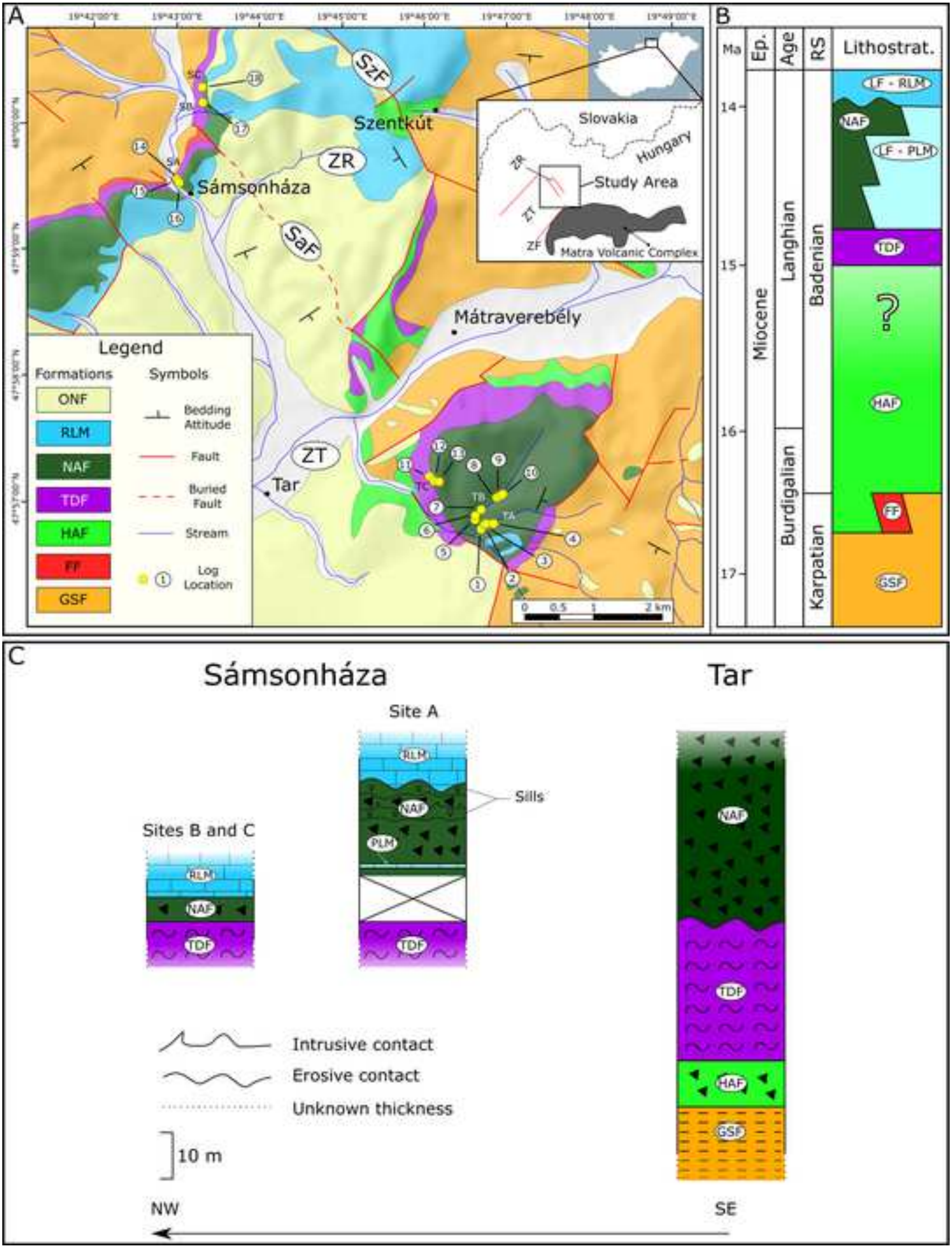
A
SzF
Szentkút
ZR
SaF
Sámsonháza
Slovakia
Hungary
Study Area
Matra Volcanic Complex
Mátraverebély
ZT
Tar
Legend
Formations
ONF
RLM
NAF
TDF
HAF
FF
GSF
Symbols
Bedding Attitude
Fault
Buried Fault
Stream
Log Location
0 0.5 1 2 km
B
Ma
Ep.
Age
RS
Lithostrat.
14
15
16
17
Miocene
Langhian
Burdigalian
Badenian
Karpatian
LF - RLM
NAF
LF - PLM
TDF
?
HAF
FF
GSF
C
Sámsonháza
Tar
Site A
Sills
Sites B and C
RLM
NAF
PLM
TDF
HAF
GSF
Intrusive contact
Erosive contact
Unknown thickness
10 m
NW
SE

Figure 2 Click here to access/download;Figure;Figure 2.jpg

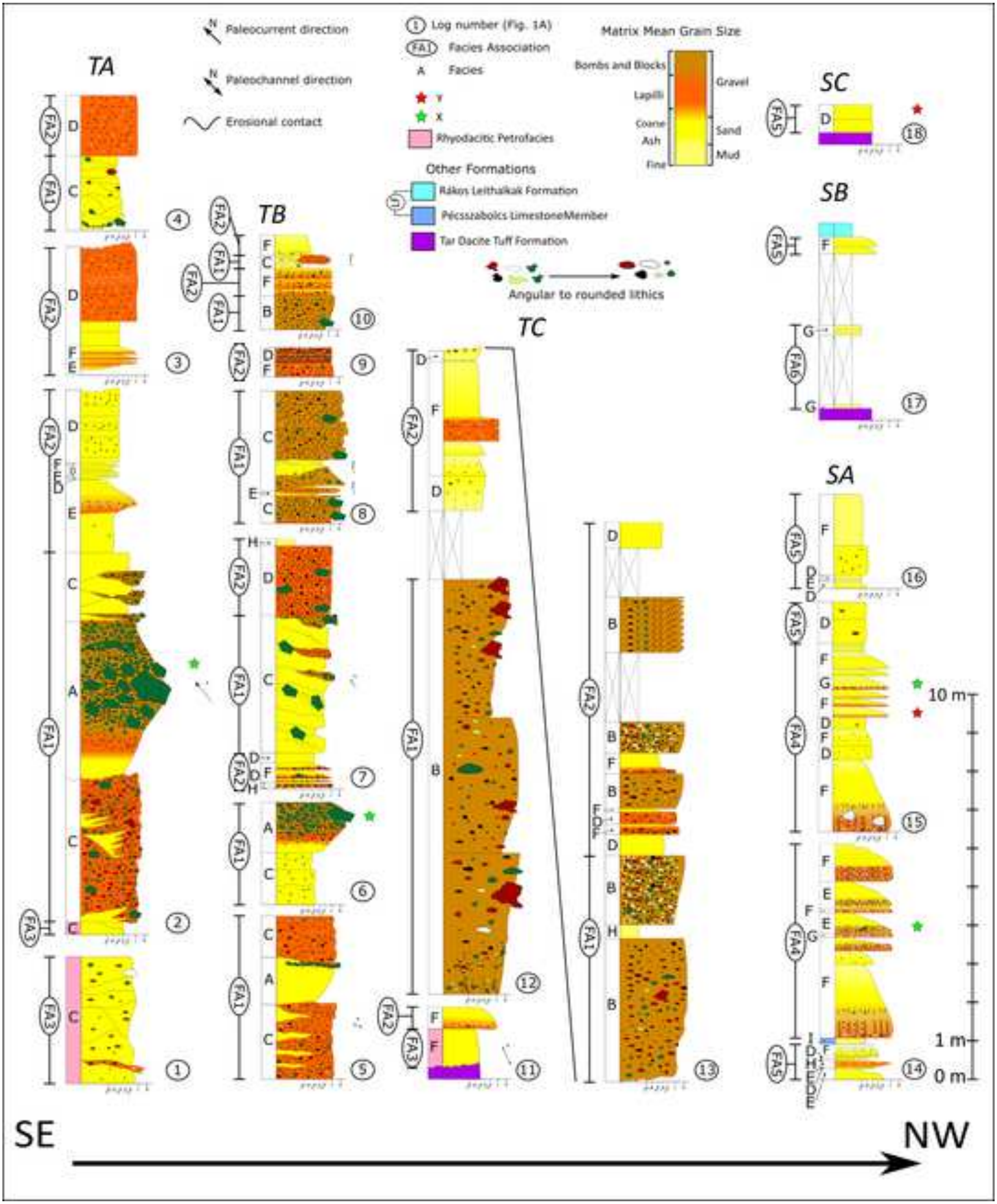

Figure 3

Click here to access/download;Figure;Figure 3.jpg

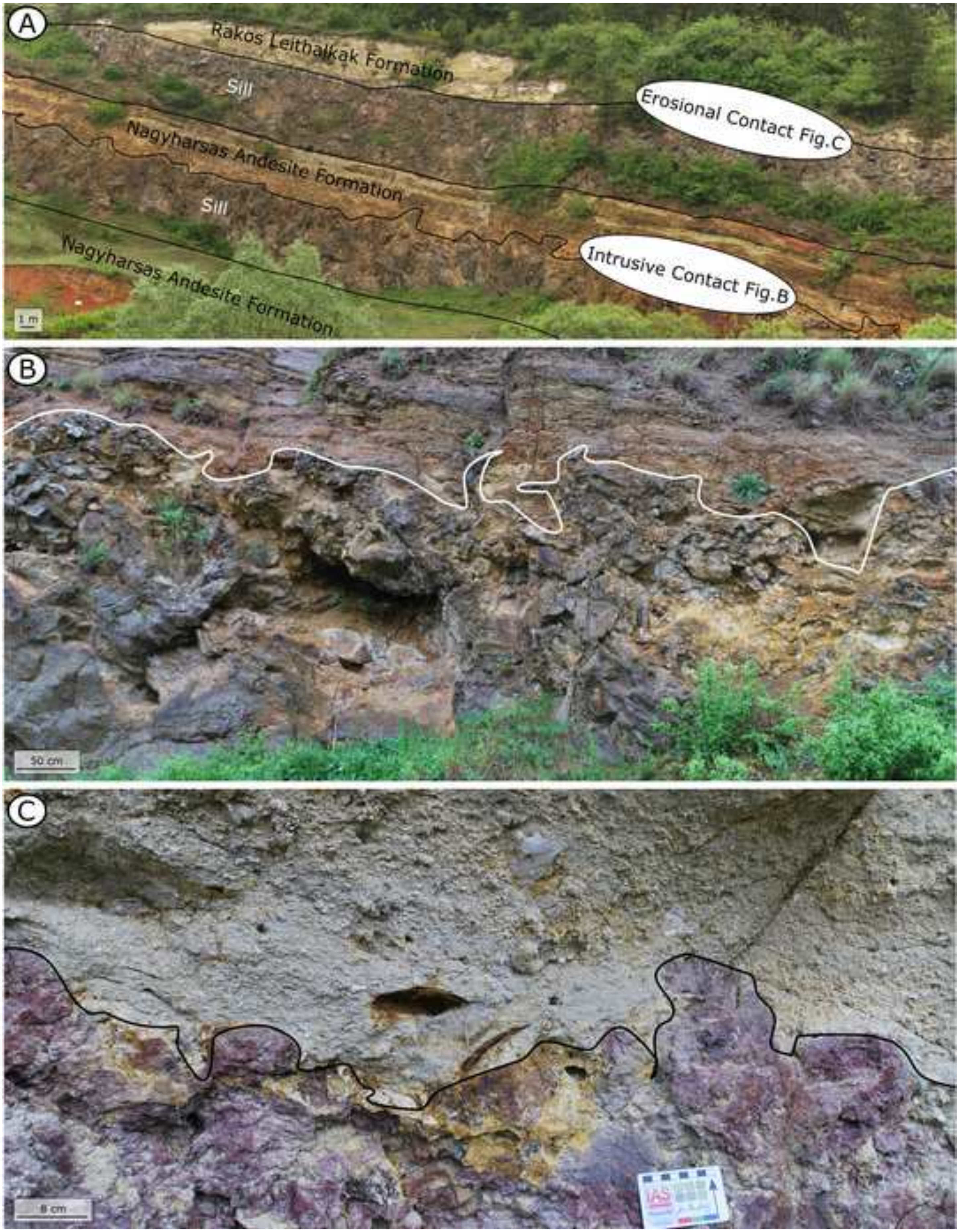

Figure 4

Click here to access/download;Figure;Figure 4.jpg

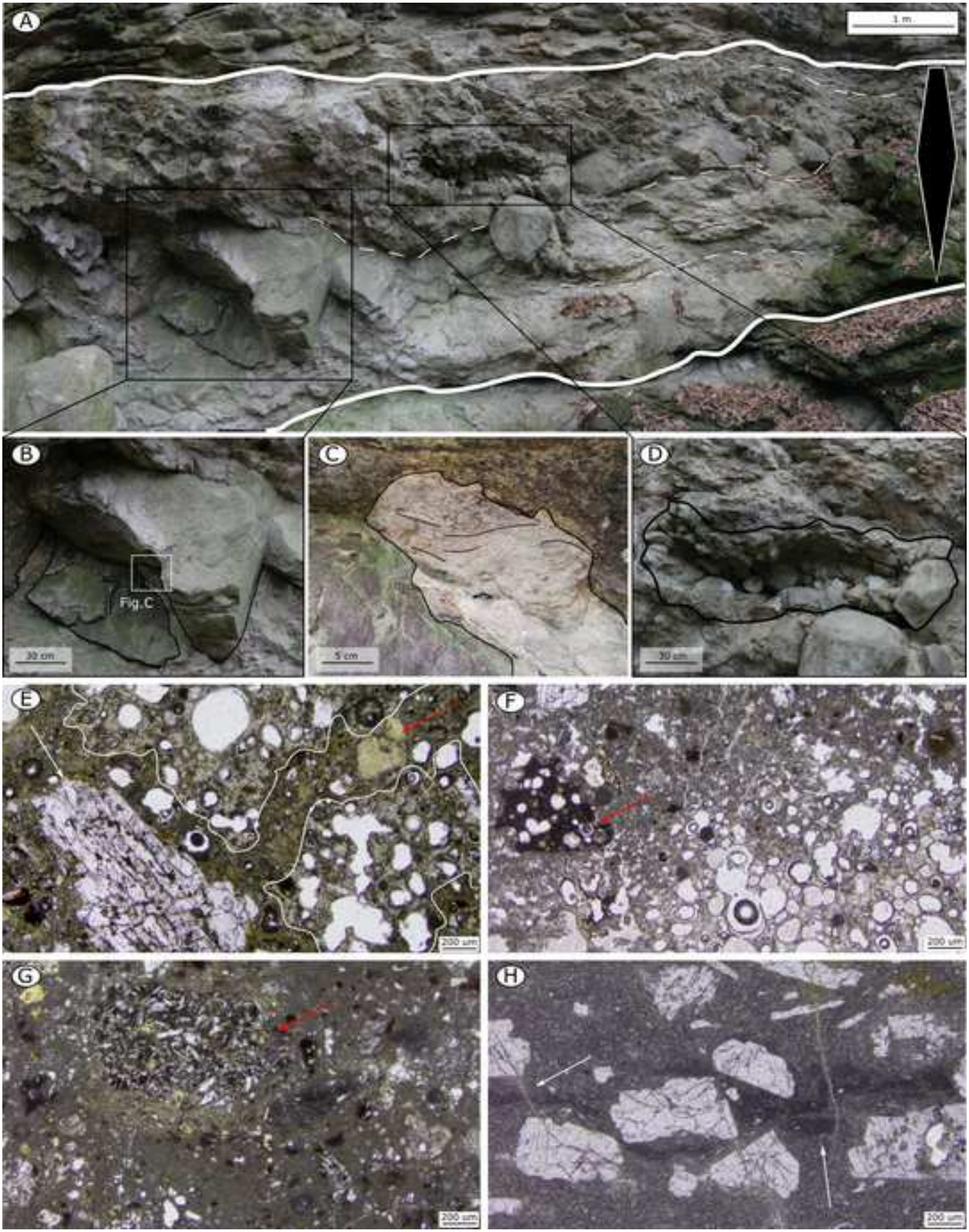

Figure 5 Click here to access/download;Figure;Figure 5.jpg

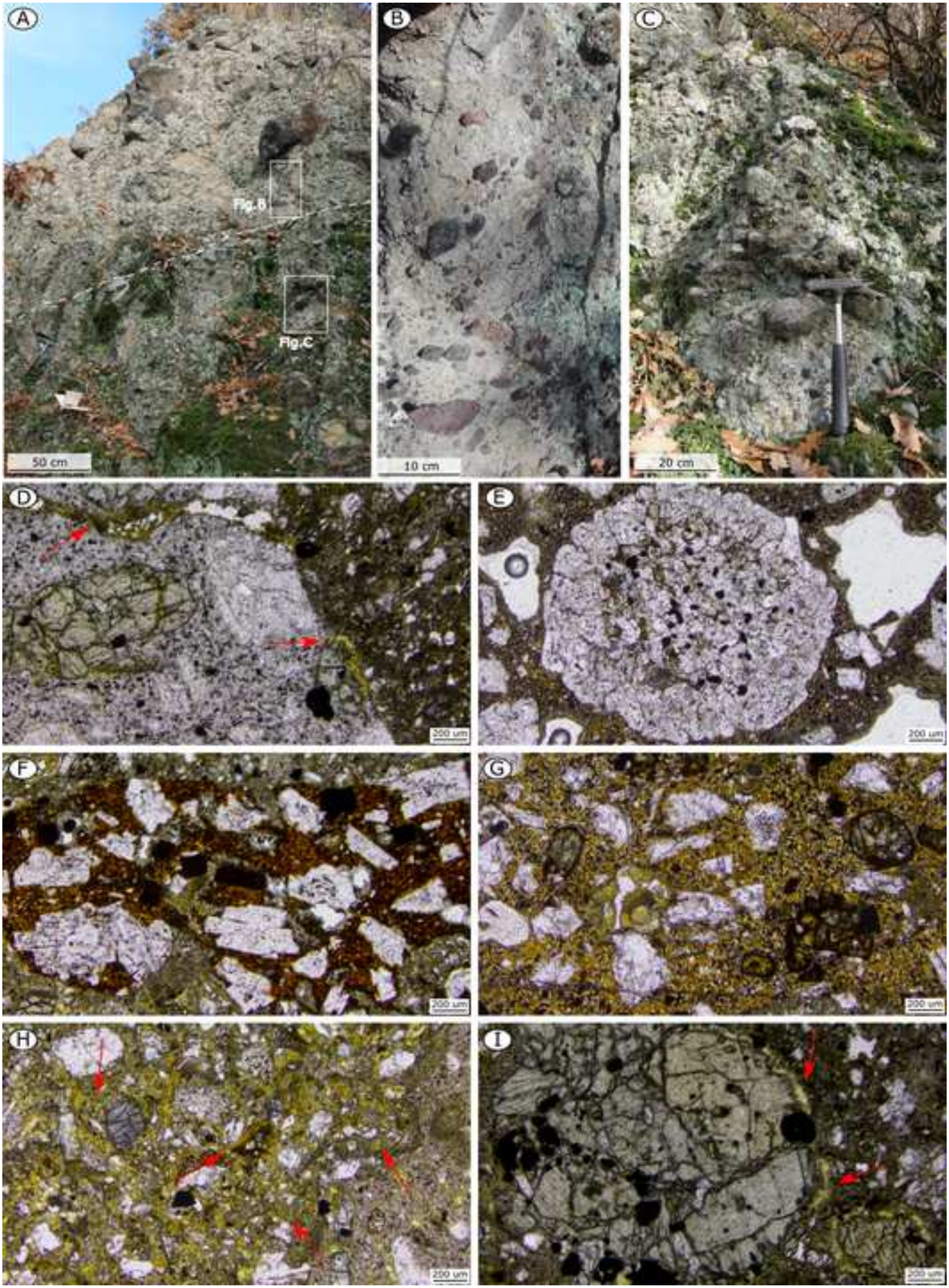

Figure 6

Click here to access/download;Figure;Figure 6.jpg

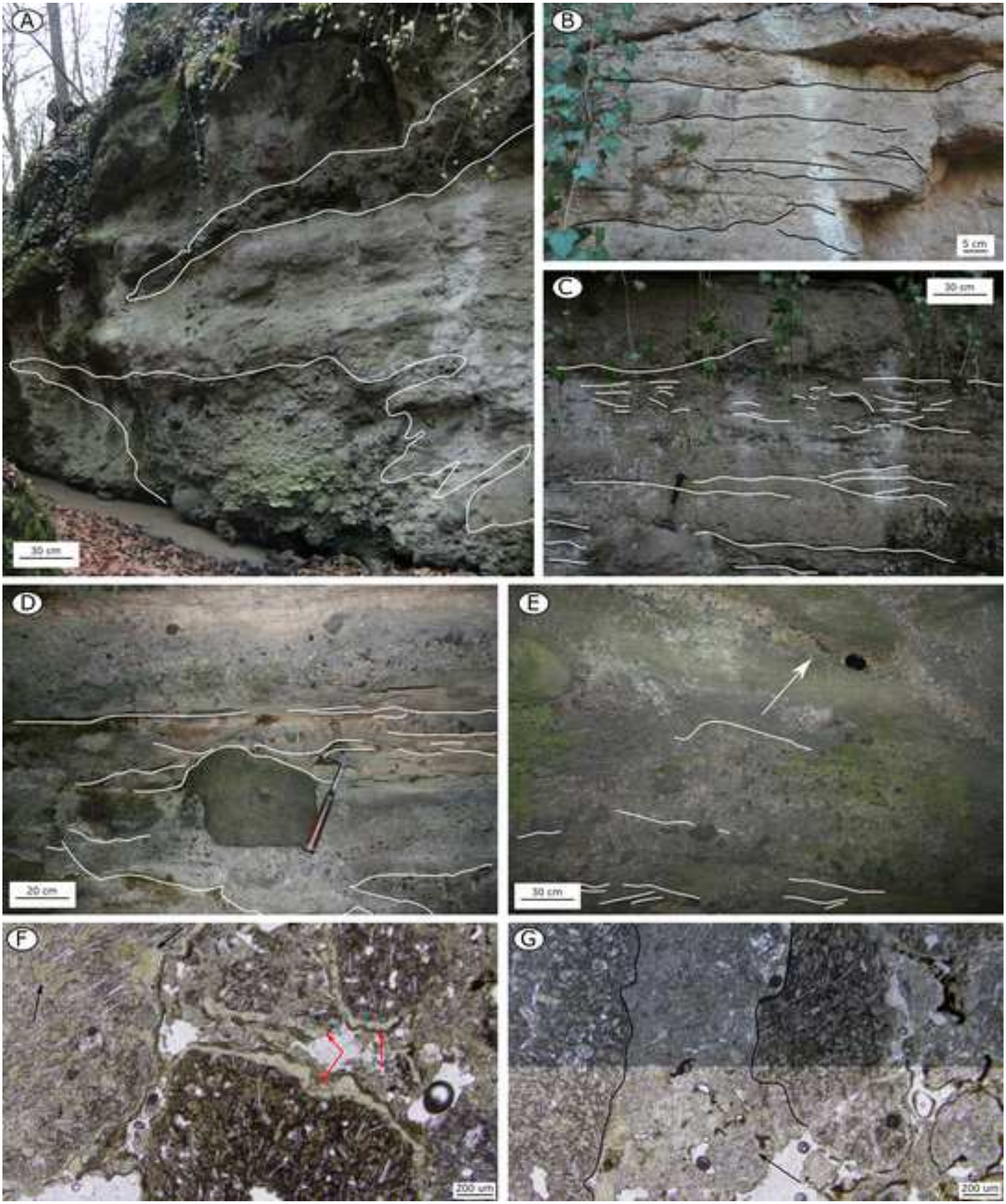

Figure 7 Click here to access/download;Figure;Figure 7.jpg

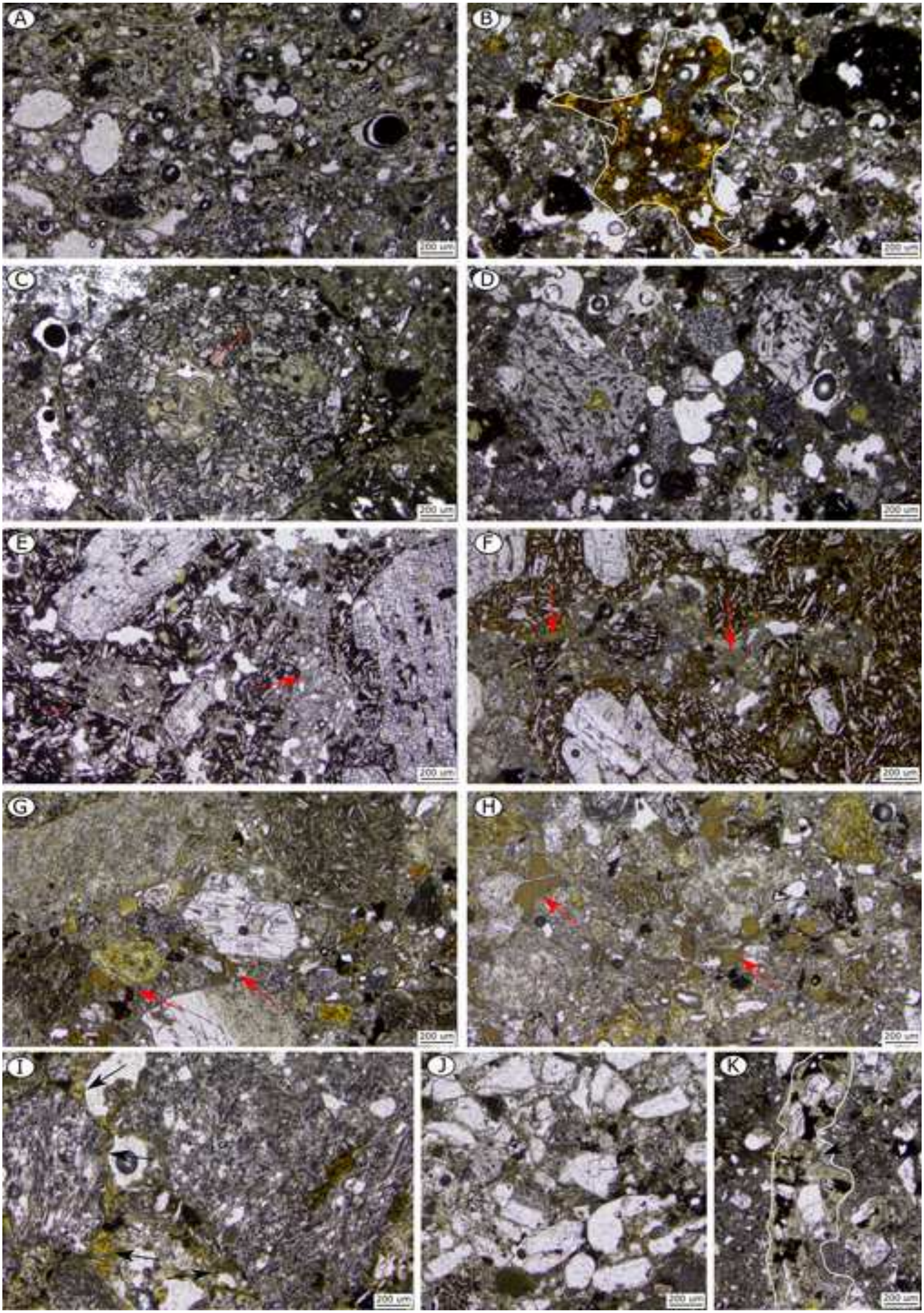

Figure 8 Click here to access/download;Figure;Figure 8.jpg

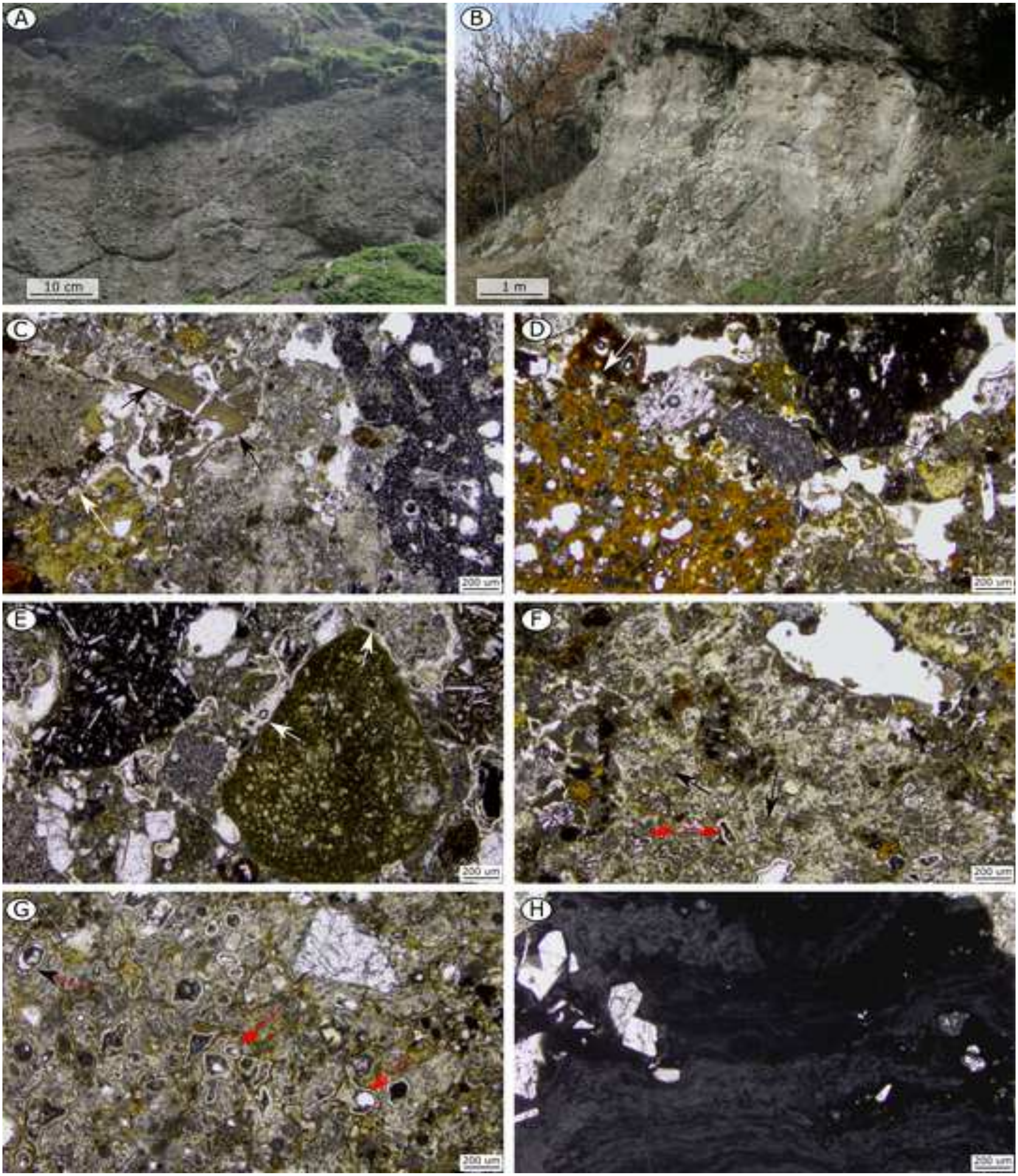

Figure 9 Click here to access/download;Figure;Figure 9.jpg

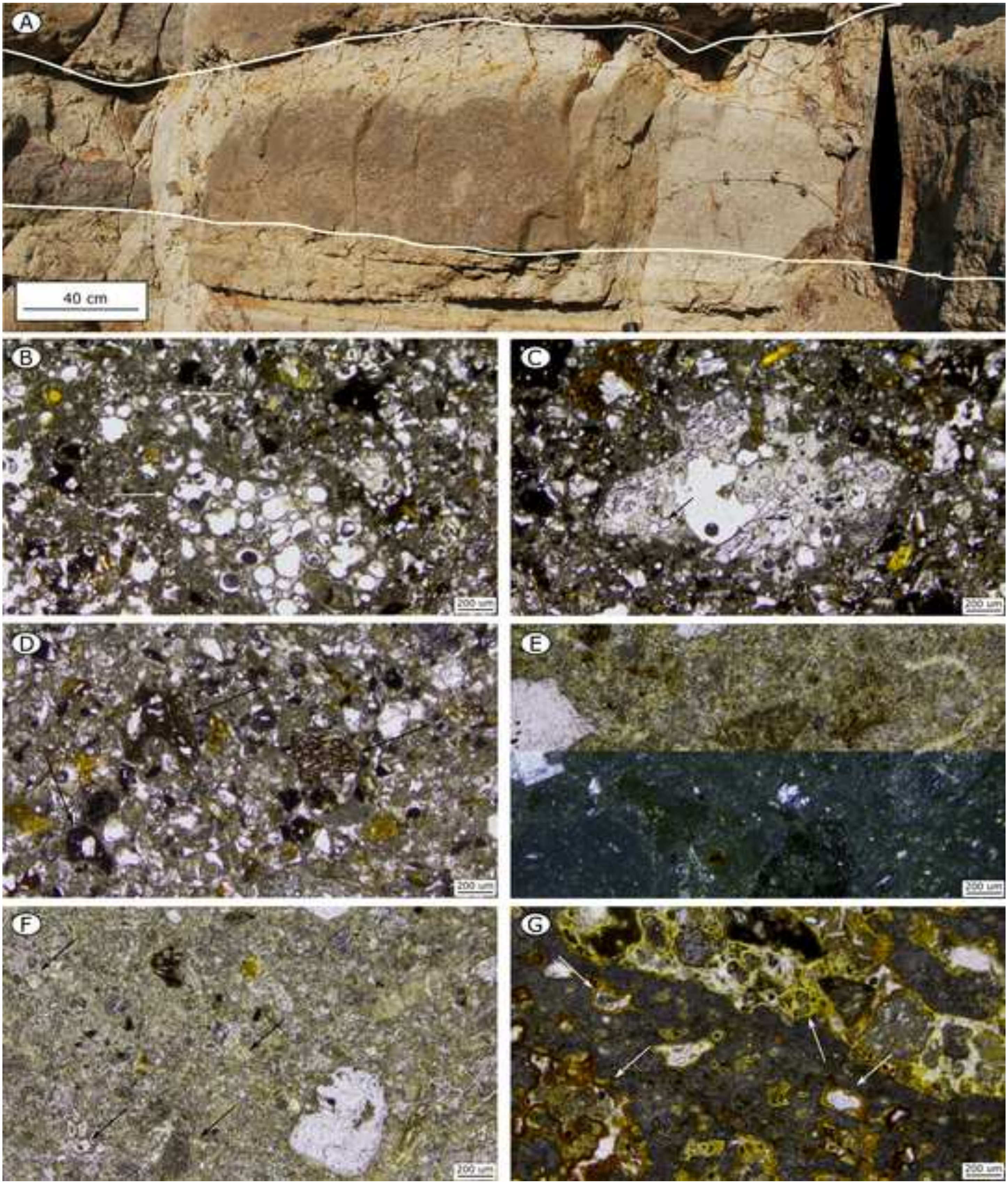

Figure 10 Click here to access/download;Figure;Figure 10.jpg

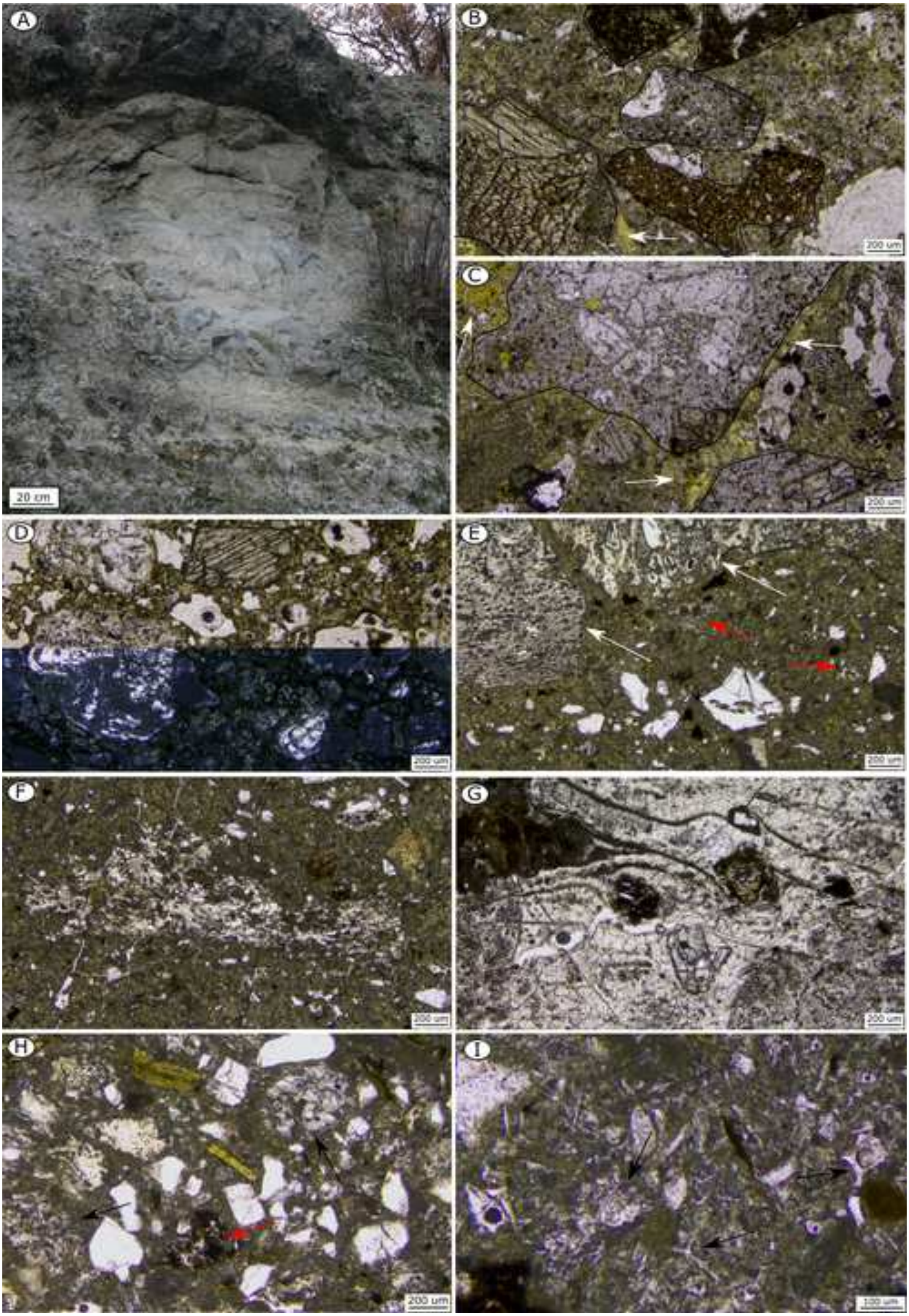

Figure 11

Click here to access/download;Figure;Figure 11.jpg

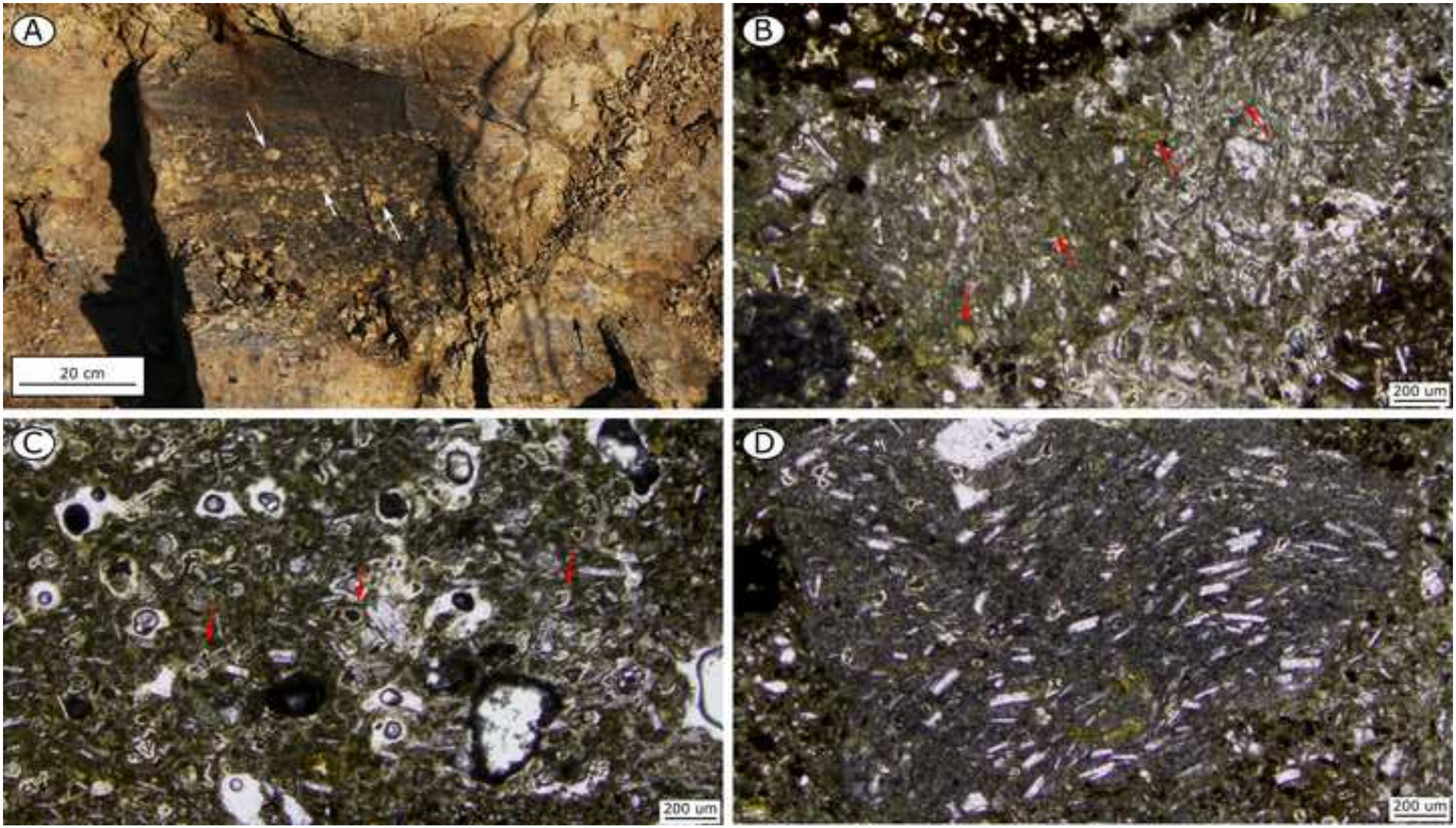

Figure 12 Click here to access/download;Figure;Figure 12.jpg

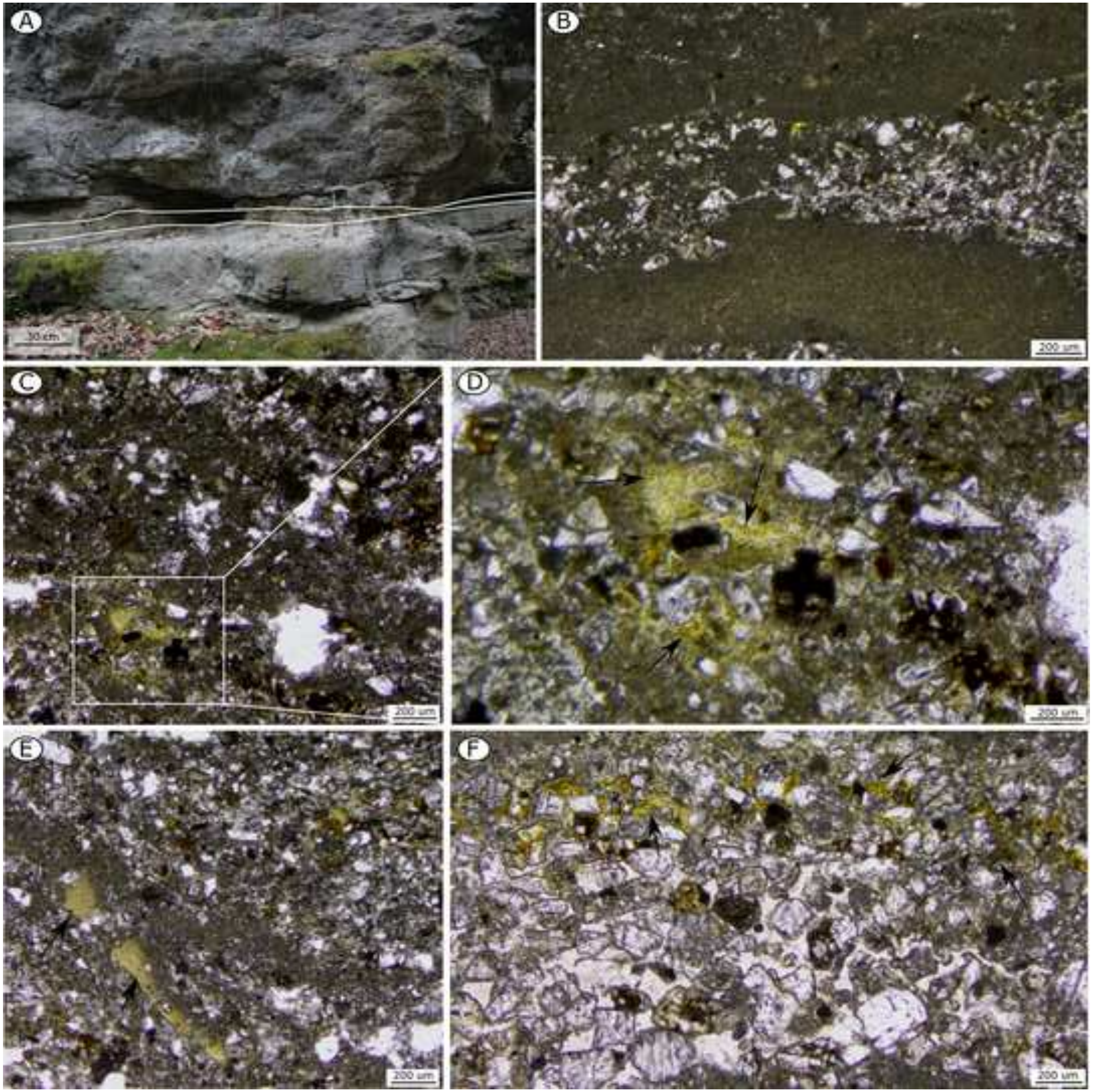

Figure 13

Click here to access/download;Figure;Figure 13.jpg

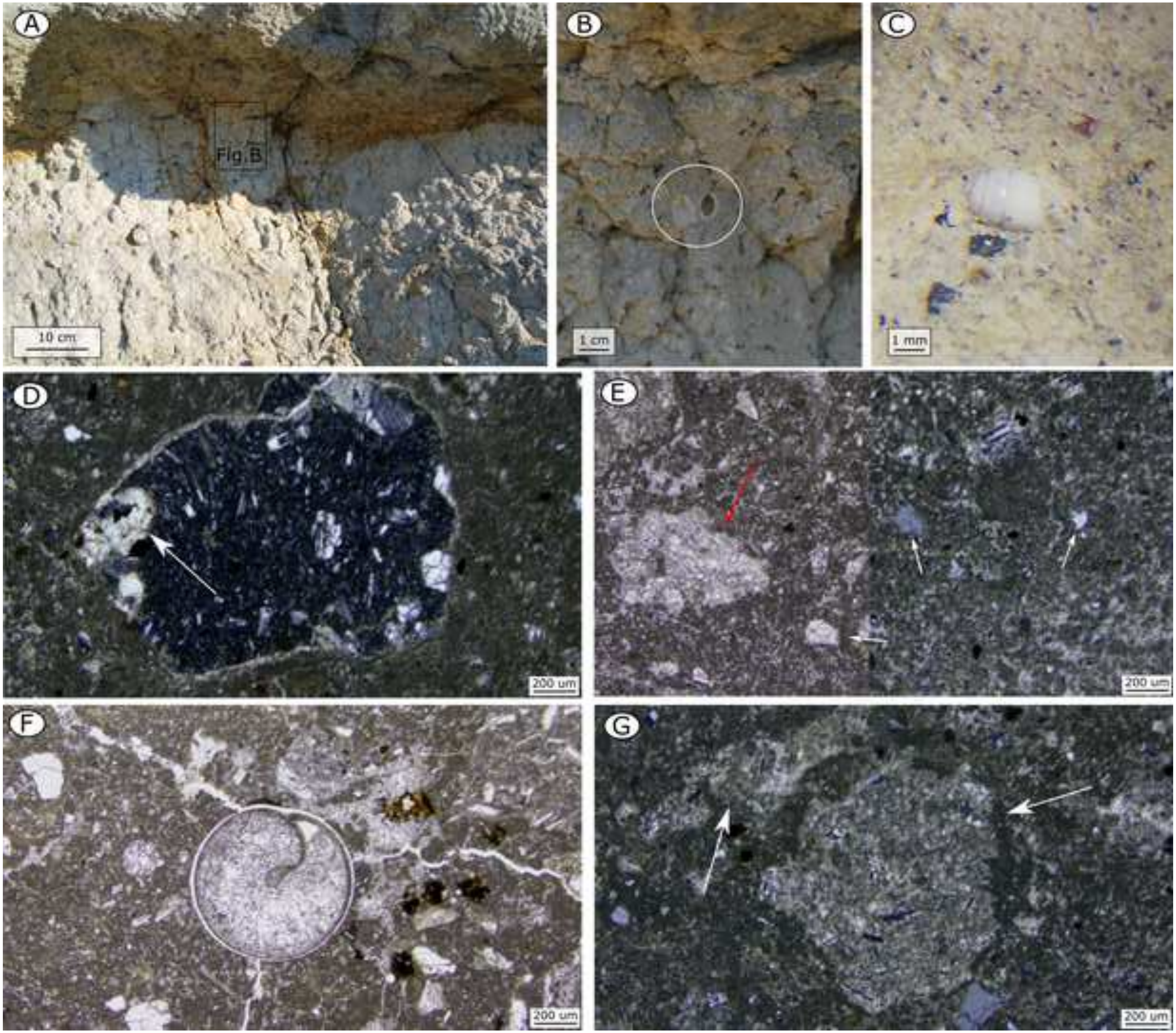

Figure 14 Click here to access/download;Figure;Figure 14.jpeg

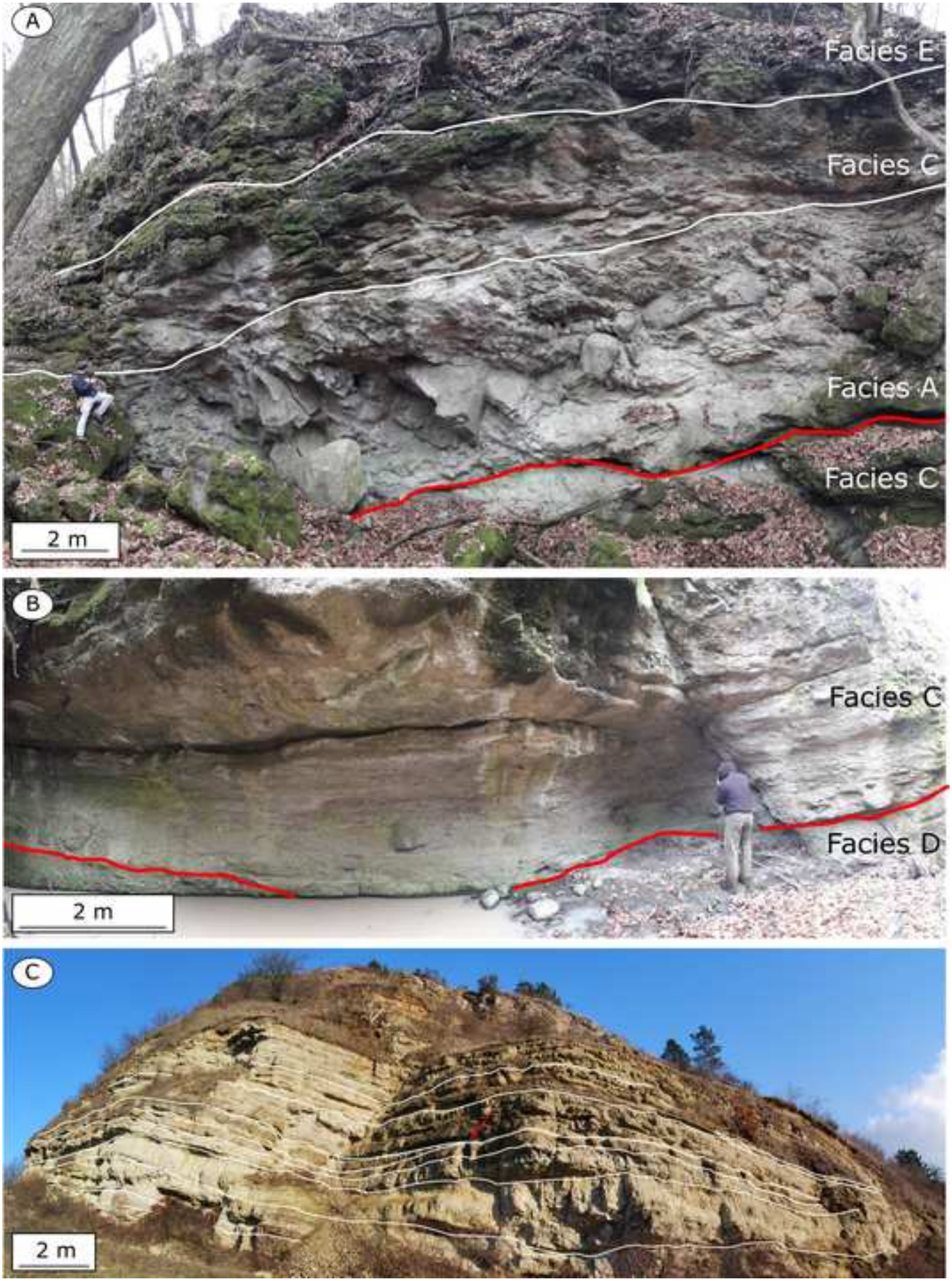

Figure 15

Click here to access/download;Figure;Figure 15.jpg

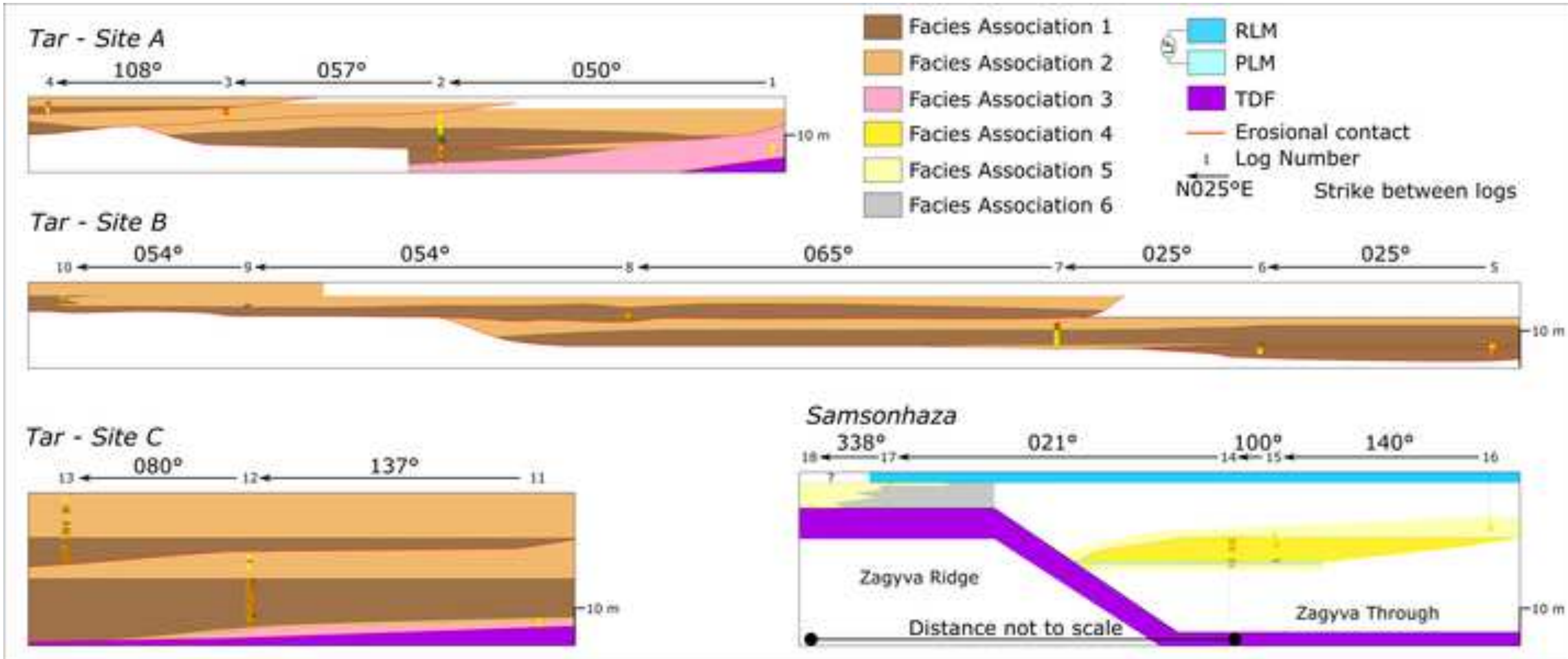

Figure 16

Click here to access/download;Figure;Figure 16.png

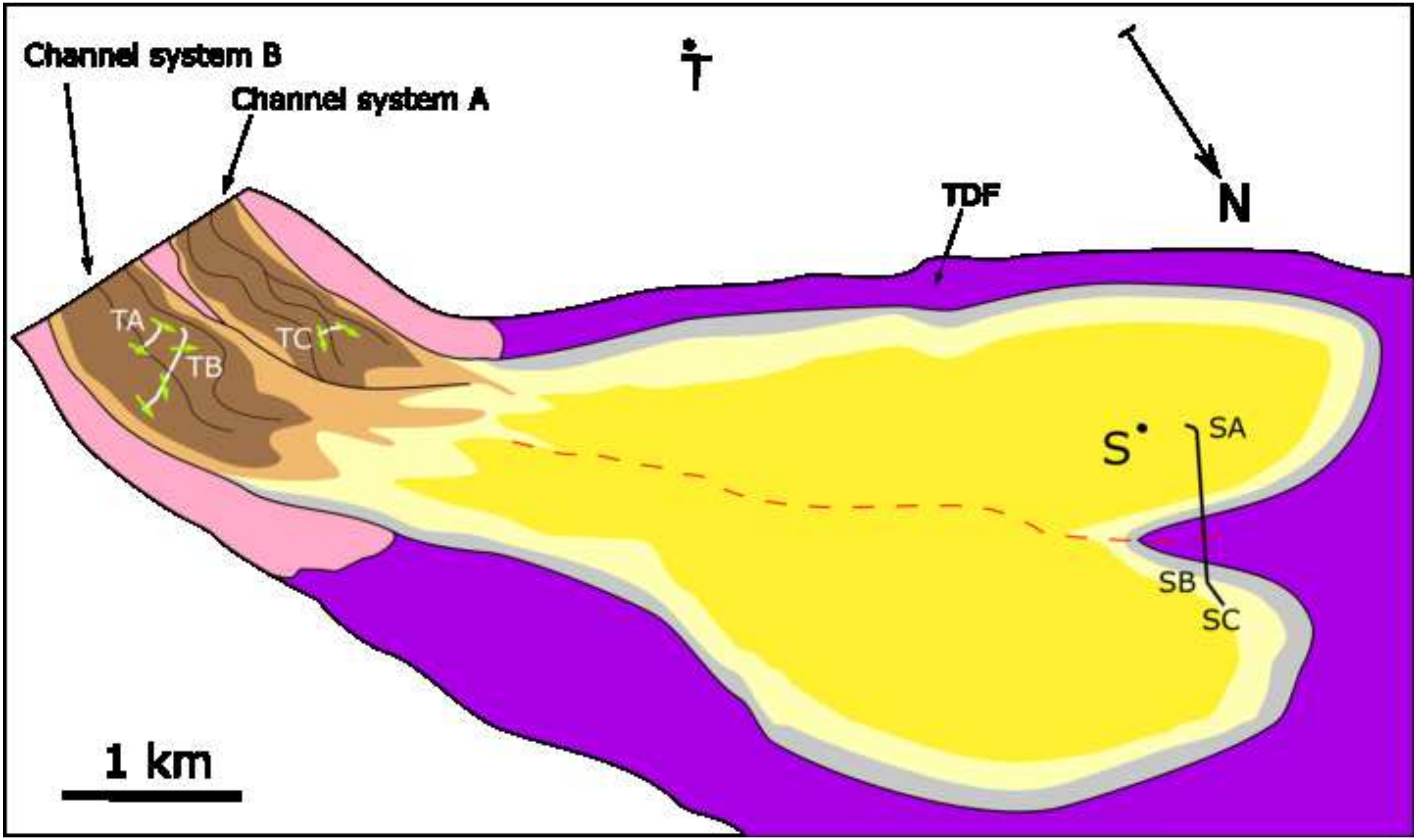

Figure 17 Click here to access/download;Figure;Figure 17.png